Atomic Data and Nuclear Data Tables xxx (xxxx) xxx

Contents lists available at ScienceDirect

Atomic Data and Nuclear Data Tables

journal homepage: www.elsevier.com/locate/adt

Astrophysical reaction rates of α-induced reactions for nuclei with $26 \leq Z \leq 83$ from the new Atomki-V2 α-nucleus potential

P. Mohr [a,*], Zs. Fülöp [a], Gy. Gyürky [a], G.G. Kiss [a], T. Szücs [a], A. Arcones [b,c], M. Jacobi [b], A. Psaltis [b]

[a] Institute for Nuclear Research (ATOMKI), H-4001 Debrecen, Hungary
[b] Institut für Kernphysik, Technische Universität Darmstadt, D-64289 Darmstadt, Schlossgartenstr. 2, Germany
[c] GSI Helmholtzzentrum für Schwerionenforschung GmbH, Planckstr. 1, D-64291 Darmstadt, Germany

ARTICLE INFO

Article history:
Received 30 April 2021
Received in revised form 11 June 2021
Accepted 9 July 2021
Available online xxxx

ABSTRACT

The new Atomki-V2 α-nucleus potential is applied to calculate astrophysical reaction rates $N_A\langle\sigma\, v\rangle$ of intermediate mass and heavy target nuclei from iron ($Z = 26$) up to bismuth ($Z = 83$). Overall, reaction rates of α-induced reactions are provided for 4359 target nuclei, covering as well neutron-deficient as extremely neutron-rich target nuclei from the proton to the neutron dripline. Contrary to previous rate compilations, these new calculations include all relevant exit channels with the dominating (α, xn) reactions for neutron-rich target nuclei.

* Corresponding author.
E-mail address: mohr@atomki.hu (P. Mohr).

https://doi.org/10.1016/j.adt.2021.101453

Please cite this article in press as: P. Mohr, Z. Fülöp, G. Gyürky et al., Astrophysical reaction rates of α-induced reactions for nuclei with $26 \leq Z \leq 83$ from the new Atomki-V2 α-nucleus potential, Atomic Data and Nuclear Data Tables (2021) 101453, https://doi.org/10.1016/j.adt.2021.101453.

Contents

1. Introduction

α-induced reactions play an essential role in various astrophysical scenarios. This starts in the big bang nucleosynthesis with lithium-producing α capture reactions (e.g., [1]) and continues in different quiescent and explosive burning phases of stars. In particular, α-capture reactions appear in the $pp-II$ and $pp-III$ chains of hydrogen burning, and they govern helium burning by the triple-alpha process and the subsequent ^{12}C(α, γ)^{16}O and ^{16}O(α, γ)^{20}Ne reactions. (α,p) reactions on light nuclei provide a path for the break-out from hot CNO cycles to the rapid proton capture process (*rp*-process), and the ^{13}C(α,n)^{16}O and ^{22}Ne(α,n)^{25}Mg reactions are the neutron sources for the slow neutron capture process (*s*-process) [2,3]. The present study focuses on α-induced reactions on intermediate mass and heavy nuclei. Here, mainly two different scenarios have been studied in the last years: (*i*) nucleosynthesis of neutron-deficient nuclei, so-called *p*-nuclei, in the astrophysical *p*-process (also called γ-process) and (*ii*) nucleosynthesis under special conditions of the rapid neutron capture process (*r*-process), typically referred to as weak *r*-process (also known as α-process).

For the first scenario (*i*), nucleosynthesis in the *p*-process (γ-process) proceeds via a series of photon-induced (γ,n), (γ,p), and (γ, α) reactions on heavy seed nuclei. The photons are provided by the thermal photon bath at sufficiently high temperatures of several billion Kelvin ($T_9 \approx 2-3$ where T_9 is the temperature in Giga-Kelvin). First, core-collapse supernovae have been suggested as its astrophysical site [4], but significant nucleosynthesis of the neutron-deficient *p*-nuclei may also occur in supernovae of type Ia (e.g., [5]). A final conclusion on the astrophysical site(s) of the *p*-process and the origin of the low-abundant *p*-nuclei is still missing. For further information, see the review papers by Lambert [6], Rauscher et al. [7], and Pignatari et al. [8], and the sensitivity study by Nishimura et al. [9]. The required (γ, α) reaction rates are best constrained by experiments on the reverse (α, γ) reaction which started with the pioneering works at Atomki by Fülöp et al. [10] and by Somorjai et al. [11]. As noticed in [11], nowadays it is generally accepted that the

calculation of (α, γ) cross sections for heavy target nuclei is mainly sensitive to the α-nucleus optical model potential (AOMP) which is chosen in the usually applied statistical model. Reaction rates of (α, γ) reactions are the first major contribution of this work.

The second above scenario (*ii*) on the role of $(\alpha$,n) reactions for the weak *r*-process was studied very recently. It was pointed out e.g. by Bliss et al. [12] that $(\alpha$,n) reactions are an alternative path under *r*-process conditions to increase the charge number Z which may be more effective than the relatively slow β^- decays. Nuclei up to silver ($Z = 47$) can be produced under these circumstances on a path which is located a few mass units "east" of stability [12]. Related papers [13,14] confirmed the relevance of the AOMP for the calculation of $(\alpha$,n) rates. A recent sensitivity study has identified some key reactions for a variety of relevant astrophysical conditions [15]; a few of these reactions were measured almost simultaneously [16,17]. Reaction rates of $(\alpha$,n) reactions are the second major contribution of this work.

In general, reaction rates of α-induced reactions are considered as highly uncertain because the predicted cross sections from the various available AOMPs differ dramatically towards lower energies, with deviations exceeding one order of magnitude. One explanation for the wide range of predictions was given in our recent paper [18], and a new AOMP, the so-called Atomki-V2 potential, was suggested in the Supplement of [18]. Predictions from the Atomki-V2 potential typically agree well with experimental data, and it was estimated in [18] that astrophysical reaction rates can be provided with significantly reduced uncertainties. It is the scope of the present paper to provide these rates to the astrophysical community.

The paper is organized as follows: In Section 2, the statistical model calculations are briefly described, and the important role of the AOMP is pointed out. Section 3 introduces the chosen code for the statistical model calculations. Detailed results are shown in Section 4 for two examples: the first example ^{188}Sm is an extremely neutron-rich isotope, located about 40 neutrons "east" of the stable samarium isotopes between ^{144}Sm and ^{154}Sm on the chart of nuclides and close to the expected *r*-process path [19]. The second example ^{88}Kr has been identified as important for the above mentioned weak *r*-process scenario [15]. A general discussion of the present approach is provided in Section 5, and finally this work is summarized in Section 6. The Appendix A lists the modifications which have been made to the TALYS code to implement the Atomki-V2 potential.

This work uses the terminus "astrophysical reaction rate" for the quantity $N_A\langle\sigma v\rangle$. Strictly speaking, the reaction rate for a given reaction (per cubic-centimeter and second) results from $N_A\langle\sigma v\rangle$ after multiplication with the densities of the colliding nuclei. The terminus "reactivity" has been suggested for $N_A\langle\sigma v\rangle$ (e.g., [20]), but this correct terminus is not yet widely used in the community.

2. Statistical model and the α-nucleus potential

2.1. Statistical model

The statistical model is a standard approach for the calculation of reaction cross sections for heavy target nuclei. It is based on the assumption that the reaction proceeds via the formation of a compound nucleus which can decay later (and independent of the formation) by emission of γ-rays, protons, neutrons, α-particles, and combinations of these ejectiles. In a very schematic notation, the cross section of an α-induced reaction (α, X) in the laboratory is given by

$$\sigma(\alpha, X) \sim \frac{T_{\alpha,0} T_X}{\sum_i T_i} = T_{\alpha,0} \times b_X \qquad (1)$$

with the transmission coefficients T_i into the *i*th open channel and the branching ratio $b_X = T_X / \sum_i T_i$ for the decay into the channel X. The total transmission is given by the sum over all contributing channels: $T_{\mathrm{tot}} = \sum_i T_i$. The T_i are calculated from global optical potentials for the particle channels and from the γ-ray strength function (GSF) for the photon channel. For further details of the definition of T_i, see [20]. In general, for heavy target nuclei and low energies, the transmission of the α-particle $T_{\alpha,0}$ in the entrance channel is much smaller than T_γ or T_n. Thus, below the neutron threshold $b_\gamma \approx 1$, and the (α, γ) cross section depends only on $T_{\alpha,0}$. Above the neutron threshold, $b_n \approx 1$, and the $(\alpha$,n) cross section depends only on $T_{\alpha,0}$. As $T_{\alpha,0}$ depends only on the chosen AOMP, experimental data for (α, γ) cross sections below the neutron threshold and for $(\alpha$,n) cross sections above the neutron threshold are appropriate to constrain the AOMP without ambiguities from other ingredients of the statistical model.

The above Eq. (1) is valid for laboratory experiments where the target nucleus is in its ground state. Thus, the transmission in the entrance channel is given by $T_{\alpha,0}$. Contrary, the high temperatures in the stellar interior lead to thermal population of excited states in the target nucleus which have to be taken into account in Eq. (1). As a consequence, under stellar conditions Eq. (1) has to be extended to take into account that excited states in the target nucleus are thermally populated, leading to an entrance channel transmission T_α instead of $T_{\alpha,0}$. But the transmissions $T_{\alpha,i>0}$ to excited states of the target nucleus are typically smaller than $T_{\alpha,0}$ to the ground state. Thus, T_α remains smaller than T_γ or T_n under typical stellar conditions because the Coulomb barrier suppresses transitions to excited states. Hence, also stellar cross sections and the resulting stellar reaction rates of α-induced reactions depend mainly on the chosen AOMP.

The astrophysical reaction rate $N_A\langle\sigma v\rangle$ is calculated by folding the thermal Maxwell–Boltzmann velocity distribution with the energy- (or velocity-) dependent cross section σ^* under stellar conditions (i.e., including thermal excitations of the target nucleus):

$$N_A\langle\sigma v\rangle = N_A \left(\frac{8}{\pi\mu}\right)^{1/2} \left(\frac{1}{kT}\right)^{3/2} \int_0^\infty \sigma^*(E) E \exp\left(-\frac{E}{kT}\right) dE \qquad (2)$$

with the Avogadro number N_A, the reduced mass μ, and the Boltzmann constant k. The full formalism for the calculation of astrophysical reaction rates $N_A\langle\sigma v\rangle$ is given e.g. in [20] or in the widely used reaction rate tables by Rauscher and Thielemann [21].

2.2. Atomki-V2 α-nucleus potential

The Atomki-V2 potential is based on the double-folding approach [22–24]. As a consequence, the number of adjustable parameters is small which allows a relatively robust extrapolation to unknown nuclei. The parameters of the Atomki-V2 potential were completely fixed in the following way (for details, see the Supplement of [18]). The basis of the Atomki-V2 potential is the Atomki-V1 potential [25] which was derived from an analysis of elastic scattering angular distributions at low energies around the Coulomb barrier. Very briefly, the Atomki-V1 potential consists of a real folding potential in combination with a phenomenological Woods–Saxon imaginary potential. It is found that the volume integrals of the real part are practically energy-independent and have a strength of $J_R = 342.4$ MeV fm^3 for semi-magic and 371.0 MeV fm^3 for non-magic nuclei; i.e., the shape of the real part of the potential is fully constrained by the folding approach, and the strength of the real potential is obtained by scaling to the above volume integrals, leading to a completely fixed real part.

The imaginary part of Atomki-V1 is energy-dependent with an increasing strength, saturating at higher energies.

Later it was pointed out that the tail of the imaginary potential at radii much larger than the colliding nuclei affects the calculated reaction cross sections at very low energies [18] which is the astrophysically relevant energy region. Unfortunately, this tail of the imaginary potential is not well constrained, e.g. by experimental elastic scattering data. This holds for all global AOMPs which are used for the calculation of astrophysical reaction rates $N_A\langle\sigma v\rangle$.

To avoid such complications with the tail of the imaginary potential, total reaction cross sections of α-induced reactions were calculated using a simple barrier transmission approach in combination with the real part of the Atomki-V1 potential which is well-constrained by experimental scattering data. Excellent agreement with experimental total reaction cross sections was found [16–18,26]. Furthermore, the simple barrier transmission approach is numerically more robust than full optical model calculations. However, the simple barrier transmission approach does not allow to calculate the cross sections of the individual exit channels like (α, γ) or (α,n).

The Atomki-V2 potential in the present study combines the parameter-free real part of the Atomki-V1 potential with a narrow, deep, and sharp-edged imaginary part of Woods–Saxon type with a depth $W_0 = 50$ MeV, radius $R = R_0 \times A_T^{1/3}$ with $R_0 = 1.0$ fm, and diffuseness $a = 0.1$ fm. This combination ensures that the total reaction cross section remains very close to the simple barrier transmission approach; typical deviations are of the order of 10% [18]. From a practical point of view, the Atomki-V2 potential can be used for statistical model calculations without major modifications of the standard codes. In the following, cross sections and astrophysical reaction rates will be calculated by a slightly modified version of the widely used computer code TALYS [27], version 1.8, which is available as open source code. A comparison to other AOMPs will be given for the chosen examples of ^{188}Sm + α and ^{88}Kr + α in Section 4. The necessary modifications to the TALYS code are listed in Appendix A.

3. TALYS calculations

The TALYS code [27] is a general-purpose code for the calculation of nuclear reaction cross sections. Its source code is available which opens the chance to make minor modifications like the implementation of the Atomki-V1 and Atomki-V2 potentials. As a minimum input, the TALYS code requires the target nucleus, the projectile, and the energy of the incident α-particle. A sample input file for ^{188}Sm + α is provided in Table A. This input file will be discussed below, and it is used for the chosen example of ^{188}Sm + α in Section 4.1.

TALYS calculates the total reaction cross section $\sigma_{\rm reac}$ of the α-induced reaction and then distributes this cross section $\sigma_{\rm reac}$ among all open channels. In particular, TALYS automatically checks whether a residual nucleus e.g. from an (α,n) reaction is populated at neutron-unbound excitation energies; in such a case, another neutron emission may lead to an (α,2n) reaction. This chain is followed until no further neutron emission is energetically allowed. Note that such chains may become very long in the case of extremely neutron-rich isotopes, thus leading to increased CPU time requirements for these calculations. The calculated cross sections are finally used to determine the astrophysical reaction rates $N_A\langle\sigma v\rangle$ as a function of temperature by integration according to Eq. (2).

In general, except for the α-nucleus optical model potential, TALYS default parameters were chosen in most cases for the present study (see Table A). The only major exception was made for the preequilibrium contribution which is switched off throughout this study. The preequilibrium contribution in TALYS is based on parametrizations which may become invalid at the low energies which are most relevant for the present study. In some cases, this parametrized preequilibrium contribution may reach or even exceed the total reaction cross section $\sigma_{\rm reac}$, thus leading to inaccurate or inconsistent results.

Other exceptions from the TALYS default settings have only marginal or even negligible influence on the calculated reaction rates. As pointed out above (see Section 2.1), the most important ingredient for the calculation of α-induced reaction rates is the AOMP. Note that the chosen γ-ray strength function (parameter *strength 1*) is the default option in TALYS-V1.8; the corresponding statement in the TALYS manual ("Default: strength 1 for incident neutrons, strength 2 for other incident particles") is unfortunately erroneous. The default automatic normalization of the γ-ray strength function to experimental data is kept as enabled; for most nuclei under study, this option has no relevance because experimental data are not available for extremely neutron-rich or neutron-deficient nuclei. The choice of equidistant binning instead of the default logarithmic binning will be explained in the Appendix (Appendix A.10).

Furthermore, all options for enhanced accuracy and low cross sections were set to the TALYS maximum values to ensure reliable results at low energies. Here the cross sections of α-induced reactions are extremely suppressed for heavy target nuclei because of the high Coulomb barrier.

Astrophysical reaction rates $N_A\langle\sigma v\rangle$ were calculated for 4359 intermediate mass and heavy nuclei between iron ($Z = 26$) and bismuth ($Z = 83$). For these nuclei, the real part of the AOMP shows only a mild dependence on the target mass A [25,28]. The underlying Atomki-V1 and Atomki-V2 potentials were adjusted to elastic scattering data at low energies for targets in the mass region with this mild A dependence. Thus, the calculated reaction rates $N_A\langle\sigma v\rangle$ should be reliable for all nuclei under study. The detailed range of nuclei under study is listed in Table 1.

The stellar reaction rates $N_A\langle\sigma v\rangle$ were calculated for a temperature grid with $\Delta T_9 = 0.05$ in the interval $0.1 \le T_9 \le 0.5$, $\Delta T_9 = 0.10$ in the interval $0.5 \le T_9 \le 1.0$, $\Delta T_9 = 0.20$ in the interval $1.0 \le T_9 \le 2.0$, $\Delta T_9 = 0.25$ in the interval $2.0 \le T_9 \le 5.0$, and $\Delta T_9 = 0.50$ in the interval $5.0 \le T_9 \le 10.0$ which is finer than the TALYS built-in grid. The calculation times for the various target nuclei varied between a few minutes (lighter nuclei, close to stability) up to several hours (heavy nuclei, extremely neutron-rich, multi-neutron emission). The calculations were run on a standard Linux-based PC (i7 CPU with 8 cores) and on a Linux-based virtual machine equipped with 48 processors. Using this equipment, it was possible to calculate all rates of the present study within about 10 days.

4. Examples ^{188}Sm + α and ^{88}Kr + α

Two examples will be discussed in more detail in the following sections: ^{188}Sm + α (Section 4.1) and ^{88}Kr + α (Section 4.2). In general, for targets on the neutron-deficient side of the chart of nuclides only few open channels like (α, γ), (α,p), and (α,2p), contribute significantly to the total reaction cross section $\sigma_{\rm reac}$. This behavior is close to the better studied stable targets where also only few dominating channels like (α, γ), (α,n), and (α,2n) are found. Contrary, extremely neutron-rich compound nuclei show a different behavior because they may decay by multiple neutron emission.

Thus, the first example of the extremely neutron-rich ^{188}Sm was chosen as an illustration for multiple neutron emission. ^{188}Sm is located about 40 neutrons "east" of the stable samarium isotopes between ^{144}Sm and ^{154}Sm. It is a semi-magic nucleus ($N = 126$) which is located on the expected nucleosynthesis

Table A
TALYS input file for the example $^{188}\mathrm{Sm}+\alpha$; for further discussion of the chosen options, see text.

Keyword	Explanation
`projectile a`	incident particle α
`element Sm`	target element Sm ($Z = 62$)
`mass 188`	mass number of target nucleus (^{188}Sm)
`energy 10.0`	incident energy (not used for astrophysical reaction rates)
`strength 1`	select γ-ray strength
`strengthM1 2`	select M1 contribution of γ-ray strength
`ldmodel 1`	select level density
`jlmomp n`	select nucleon optical model potential
`alphaomp 9`	select α optical model potential: 9 = Atomki-V2 (TALYS-extension)
`transpower 20`	enhance accuracy for transmissions T_i
`xseps 1.e-30`	set low limit for cross sections
`transeps 1.e-30`	set low limit for transmissions T_i
`popeps 1.e-30`	set low limit for multiple-particle emission
`widthfluc y`	enable width fluctuation corrections
`widthmode 1`	select model for width fluctuation correction
`preequilibrium n`	switch off preequilibrium
`bins 80`	enhance bins in excitation energy
`equidistant y`	use linear binning
`astro y`	calculate astrophysical reaction rate $N_A\langle\sigma v\rangle$

path in the *r*-process [19]. The general arguments in the following discussion of ^{188}Sm + α would be similar for most neutron-rich targets in Table 1.

The second example of ^{88}Kr is located relatively close to stability. Experimental cross sections of ^{88}Kr + α may become into reach in the near future and should be compared to the predictions of this work. The ^{88}Kr(α,n)^{91}Sr reaction was identified as one of the most important reactions for weak *r*-process scenarios. Table II of [15] shows that this reaction affects the outcome of most tracers in that study.

Because of missing experimental data it is impossible for both chosen examples ^{188}Sm and ^{88}Kr to compare the predictions of this work from the Atomki-V2 potential to experimental data. Comparisons of the present approach to experimental data were provided for a series of heavy nuclei with $A > 150$ in [18]. For the weak *r*-process scenario, it was shown that the present approach outperforms other global AOMPs for ^{96}Zr [16] and for ^{100}Mo [17]. Other experimental data which reach the Gamow window with sufficient accuracy are very scarce.

4.1. Details for the example ^{188}Sm + α

4.1.1. Role of different (α, *X*) exit channels

In a first calculation, the (α, *X*) cross sections of the different exit channels were calculated. The result is shown as astrophysical S-factor in Fig. 1. According to TALYS, multiple neutron emission channels dominate, leading mainly to the production of several gadolinium isotopes between ^{186}Gd and ^{189}Gd by (α,3n), (α,4n), (α,5n), and (α,6n) reactions.

Because of missing experimental data, it must remain an open question whether these TALYS predictions for the various exit channels are really reliable. Furthermore, a mild staggering is seen in the excitation functions e.g. of the (α,2n) and (α,3n) reactions which does not look very convincing. Such staggering typically results from an insufficiently fine energy grid in the exit channels. A simple reduction of this staggering is not possible because the TALYS calculations were already made with the maximum accuracy settings. As the staggering mainly affects weak channels, no attempts have been made to modify the TALYS source code for further enhanced accuracy settings (see also Appendix A.5). Such a change would also lead to an increase of the required computing times. As the reaction rates $N_A\langle\sigma v\rangle$ are calculated by integration over the cross sections, the staggering shows only minor influence on the calculated reaction rates.

The calculated branching towards the various decay channels of the compound nucleus ^{192}Gd depends on many ingredients of

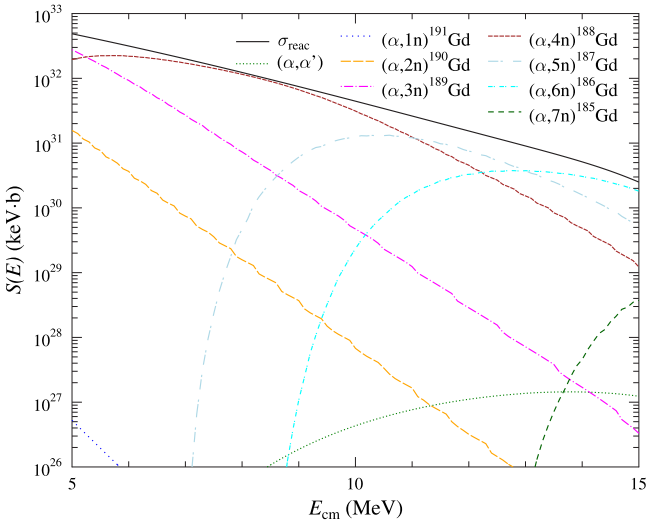

Fig. 1. Astrophysical S-factor of ^{188}Sm(α, *X*) for different exit channels. Multiple neutron emission channels like (α,3n), (α,4n), (α,5n), and (α,6n) are dominating. The full black line indicates the S-factor for the total α-induced reaction cross section σ_{reac}. Further discussion see text.

the statistical model; the branchings are most sensitive to the reaction *Q*-values and the level densities. As the *Q*-values have to be derived from global mass formulae, there are noticeable uncertainties in the *Q*-values of extremely neutron-rich nuclei. As a consequence, the calculated branching ratios should be considered as a reasonable estimate with significant uncertainties. Contrary to the branching ratios, the summed production cross section of gadolinium ($Z \rightarrow Z + 2$) is given by the sum over all (α, *x*n) reactions which is practically almost the same as the total α-induced reaction cross section; thus, the $Z \rightarrow Z+2$ production cross section of Gd depends only on the chosen AOMP.

As already pointed out above, all neutron-rich target nuclei show a qualitatively similar behavior with dominating multiple neutron emission in (α, *x*n) reactions (with $x > 1$). Obviously, the number of emitted neutrons increases towards more neutron-rich targets. E.g., for ^{170}Sm + α, we find dominating contributions to the total reaction cross section from the (α,2n) and (α,3n) reactions. For the detailed example of ^{188}Sm + α, this changes to (α,3n) to (α,6n), and for ^{200}Sm + α the dominating channels are the (α,8n) to (α,14n) reactions.

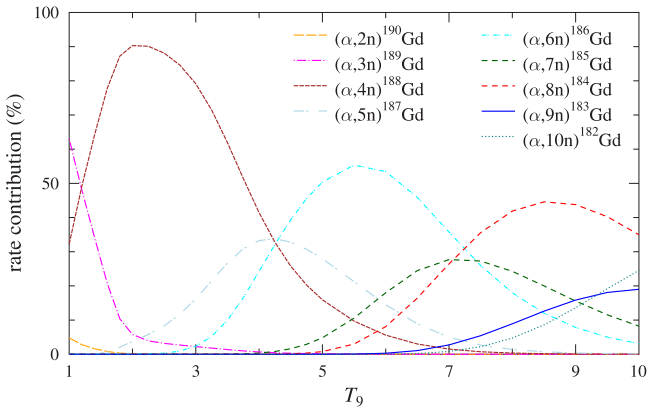

Fig. 2. Contributions of the different (α, X) exit channels to the astrophysical production rate $N_A\langle\sigma v\rangle$ of gadolinium $(Z \rightarrow Z+2)$ from ^{188}Sm(α, X) reactions as a function of temperature. Multiple neutron emission channels like $(\alpha,3n)$, $(\alpha,4n)$, $(\alpha,5n)$, and $(\alpha,6n)$ are dominating. See the text for a more detailed discussion.

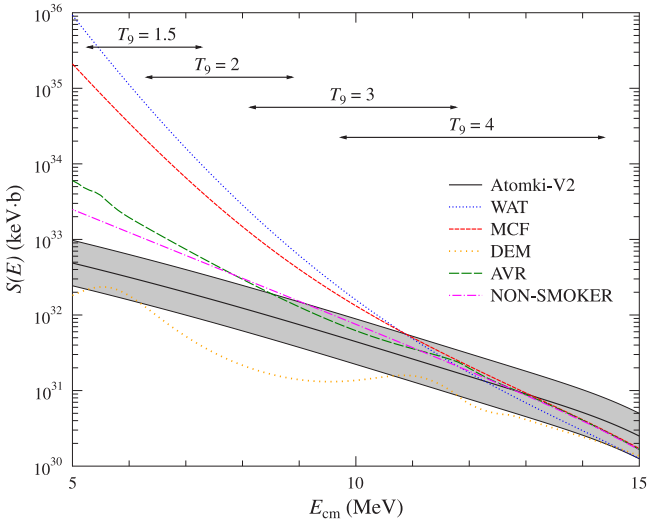

Fig. 3. Comparison of the total reaction cross section σ_{reac} of ^{188}Sm + α (shown as astrophysical S-factor) for different AOMPs. The gray-shaded region represents the estimated uncertainty of a factor of two for the Atomki-V2 prediction. The other AOMPs are taken from Watanabe (WAT) [29], McFadden and Satchler (MCF) [30], Demetriou et al. (DEM) [31], and Avrigeanu et al. (AVR) [32]. The arrows indicate the classical Gamow window for different temperatures. Further discussion see text.

Fig. 2 shows the contributions of the various (α, X) channels to the total production rate $N_A\langle\sigma v\rangle$ of gadolinium as a function of temperature. Below $T_9 = 3$, the dominating channel is the ^{188}Sm$(\alpha,4n)^{188}$Gd reaction with a significant contribution of the ^{188}Sm$(\alpha,3n)^{189}$Gd reaction around $T_9 \approx 1$. Above $T_9 = 4$ the ^{188}Sm$(\alpha,5n)^{187}$Gd and ^{188}Sm$(\alpha,6n)^{186}$Gd reactions become most important. Interestingly, the summed gadolinium production rate $(Z \rightarrow Z+2)$ is the astrophysically most relevant quantity because such neutron-rich nuclei like ^{188}Sm or ^{192}Gd are typically produced in (n, γ)-(γ,n) equilibrium under r-process conditions. As the total gadolinium production rate depends only on the AOMP and the chosen Atomki-V2 potential is typically able to reproduce (α, X) cross sections with deviations far below a factor of two [18], the calculated total gadolinium production rate should also be reliable within a factor of two. Larger uncertainties have to be assigned to the individual (α, X) rates.

4.1.2. Comparison of different α-nucleus potentials

The total reaction cross section σ_{reac} for ^{188}Sm(α, X) from the Atomki-V2 potential is compared to the predictions of various AOMPs from literature in Fig. 3. Similar to Fig. 1, for better visibility the cross sections have been converted to astrophysical S-factors. The following comparison includes the AOMPs by Watanabe (WAT; TALYS option 1) [29], McFadden and Satchler (MCF; TALYS option 2) [30], Demetriou et al. (DEM; third version; TALYS option 5) [31], and Avrigeanu et al. (AVR; TALYS option 6) [32].

Fig. 3 shows that the WAT and MCF AOMPs have a trend to a steep increase of the S-factor towards lower energies. It is well-known that these AOMPs show a general overestimation of low-energy cross sections for stable targets, e.g. found for the ^{144}Sm$(\alpha, \gamma)^{148}$Gd reaction [11,33]. Contrary to the WAT and MCF AOMPs which show a steep and monotonic increase of the S-factor towards low energies, the DEM and AVR AOMPs show a weaker, but sometimes non-monotonic energy dependence for the S-factor of the total reaction cross section σ_{reac} which is not observed experimentally (see e.g. Fig. 2 of [18]). The prediction from the DEM AOMP remains below the Atomki-V2 calculation. The AVR AOMP shows a steeper energy dependence than Atomki-V2 and predicts somewhat higher cross sections at low energies, but lower cross sections at higher energies in the energy range of Fig. 3. Both, the DEM and AVR AOMPs remain close to the estimated uncertainty range of a factor of two for the Atomki-V2 potential [18]. At the lowest energy of 5 MeV, the predictions differ by almost 4 orders of magnitude between the highest value (WAT) and the lowest value (DEM). Finally, the NON-SMOKER cross sections, taken from the web page of [34], are quite close to the predictions of the AVR AOMP. This is somewhat surprising as the NON-SMOKER cross sections are based on the MCF AOMP. Technical differences between widely used statistical model codes have been investigated in [35], and it was found that these so-called "non-model effects" have a non-negligible effect on neutron capture cross sections. However, these "non-model effects" should be very marginal in the present case of total α-induced cross sections σ_{reac} as shown in Fig. 3 (and later for ^{88}Kr in Fig. 7) because σ_{reac} results from a pure optical model calculation and is independent of all technical details of the treatment of the statistical model.

The horizontal arrows in Fig. 3 indicate the astrophysically most relevant energies for ^{188}Sm + α for temperatures of $T_9 = 1.5$, 2, 3, and 4, the so-called standard Gamow window. However, as pointed out by Rauscher [36], the standard calculation of the Gamow window is somewhat misleading for heavy target nuclei because the energy dependence of the S-factor typically shifts the real Gamow window down by about $1 - 2$ MeV.

Fig. 4 shows the astrophysical reaction rates $N_A\langle\sigma v\rangle$ for the $Z \rightarrow Z+2$ production of gadolinium from ^{188}Sm + α. As expected from the S-factors in Fig. 3, the rates from the WAT and MCF AOMPs exceed the present rate dramatically at low temperatures below $T_9 \approx 3$, whereas the rates from the DEM and AVR AOMPs remain relatively close to the present rate at all temperatures with deviations below one order of magnitude.

For completeness, we study the rates from the widely used NON-SMOKER(web) code [34] and the rates from the REACLIB [37] and STARLIB [38] compilations. The rate from NON-SMOKER(web) is lower than the present rate except for the lowest temperatures. The NON-SMOKER(web) rate is also much lower than the rate from the MCF AOMP. Again, this is somewhat surprising because the NON-SMOKER(web) calculations are also based on the MCF AOMP. The REACLIB rate is also based on NON-SMOKER [21]. As expected, there is good agreement between REACLIB and NON-SMOKER(web) above $T_9 \approx 3$. However, towards lower temperatures an increasing discrepancy appears

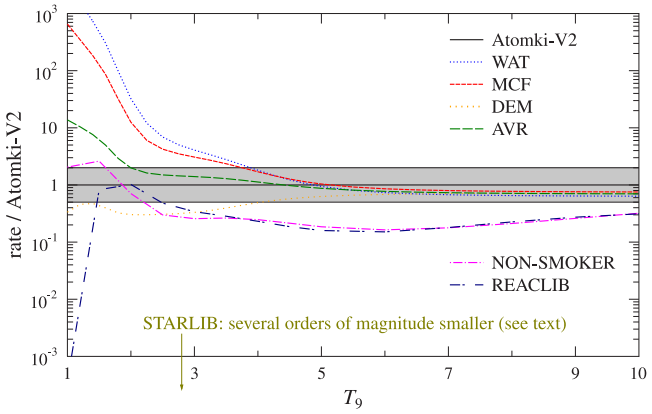

Fig. 4. Astrophysical reaction rates for the $Z \rightarrow Z+2$ production of gadolinium from ^{188}Sm + α from different AOMPs, normalized to the result of the present work. (For references, colors, and linestyles see the previous Fig. 3). In addition, the rates from NON-SMOKER(web) [34] and REACLIB [37] are included. The STARLIB [38] rate is almost 10 orders of magnitude lower and thus not shown. See the text for a more detailed discussion.

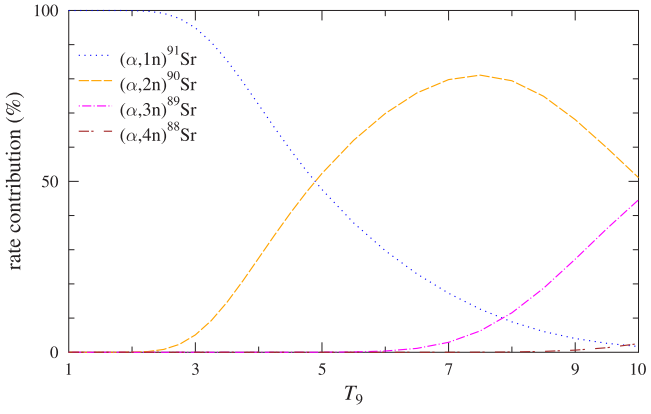

Fig. 6. Contributions of the different (α, X) exit channels to the astrophysical production rate $N_A\langle\sigma v\rangle$ of strontium ($Z \rightarrow Z+2$) from ^{88}Kr(α, X) reactions as a function of temperature. Up to $T_9 \approx 3$, the (α,1n) channel dominates. At higher temperatures the (α,2n) channel becomes dominant whereas multiple neutron emission like (α,3n) or (α,4n) appears only at extreme temperatures above $T_9 \approx 8$. See the text for a more detailed discussion.

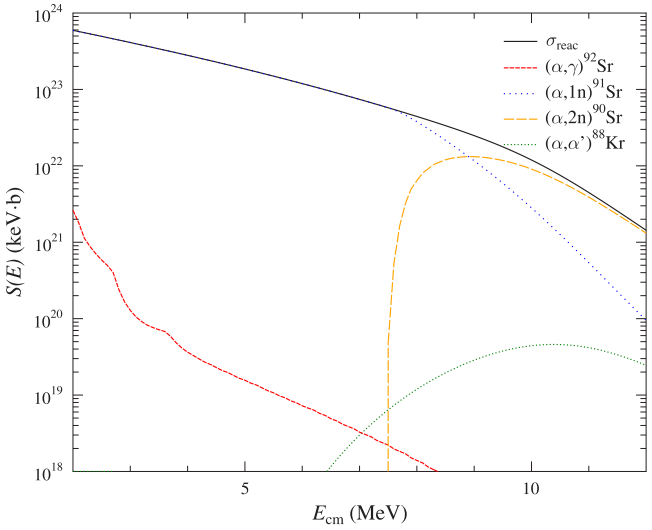

Fig. 5. Astrophysical S-factor of ^{88}Kr(α, X) for different exit channels. Up to about 8 MeV, the (α,1n) channel dominates; at higher energies, the (α,2n) channel becomes more important. The (α, γ) channel remains practically negligible. The full black line indicates the S-factor for the total α-induced reaction cross section σ_{reac}. See the text for a more detailed discussion.

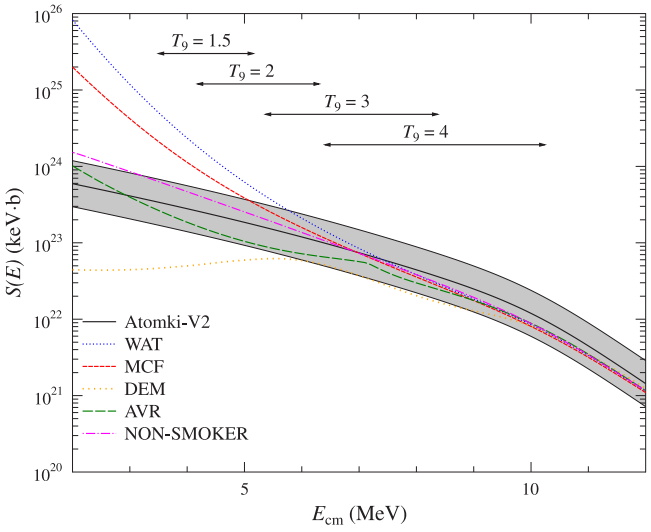

Fig. 7. Comparison of the total reaction cross section σ_{reac} of ^{88}Kr + α (shown as astrophysical S-factor) for different AOMPs. The gray-shaded region represents the estimated uncertainty of a factor of two for the Atomki-V2 prediction. The other AOMPs are taken from Watanabe (WAT) [29], McFadden and Satchler (MCF) [30], Demetriou et al. (DEM) [31], and Avrigeanu et al. (AVR) [32]. The arrows indicate the classical Gamow window for different temperatures. See the text for a more detailed discussion.

between the parametrized REACLIB rate and the tabular rate of NON-SMOKER(web); this discrepancy most likely results from the fitting procedure.

It has to be pointed out that the NON-SMOKER(web) and REACLIB rates are given as ^{188}Sm(α,n)^{191}Gd rates. NON-SMOKER does not follow the multiple neutron emission channels of the compound nucleus ^{192}Gd, and thus in fact the ^{188}Sm(α,n)^{191}Gd rates from NON-SMOKER and REACLIB are inclusive $Z \rightarrow Z+2$ rates. Contrary, the STARLIB rate, also labeled with ^{188}Sm(α,n)^{191}Gd, is indeed the rate for the production of ^{191}Gd from ^{188}Sm(α,1n)^{191}Gd. As a consequence, the STARLIB rate for ^{188}Sm(α,n)^{191}Gd is almost 10 orders of magnitude below the present rate and cannot be seen in Fig. 4.

4.2. Details for the example ^{88}Kr + α

The above procedure for ^{188}Sm + α was repeated for the second example of ^{88}Kr + α. Fig. 5 shows that the (α,1n) channel dominates already close above the threshold ($Q_{(\alpha,n)} = -1.69$ MeV) over a wide energy range up to about 8 MeV. Here the (α,2n) channel becomes more important than (α,1n). Other channels like e.g. (α, γ) remain negligible. Consequently, the $Z \rightarrow Z+2$ production rate of strontium from ^{88}Kr + α is also dominated by the (α,1n) contribution. Only at very high temperatures above $T_9 = 5$ the (α,2n) contribution exceeds the (α,1n) channel (see Fig. 6).

The influence of the chosen AOMP on the total α-induced reaction cross section σ_{reac} is shown in Fig. 7. Similar to the previous example ^{188}Sm, the WAT and MCF AOMPs show the trend to significantly increasing S-factors towards low energies. The DEM AOMP shows much lower cross sections at low energies, and the AVR AOMP remains close to the present approach over the whole energy range of Fig. 7. The predictions of the various AOMPs span a range of more than three orders of magnitude at 2 MeV; however, the astrophysically relevant energy region is

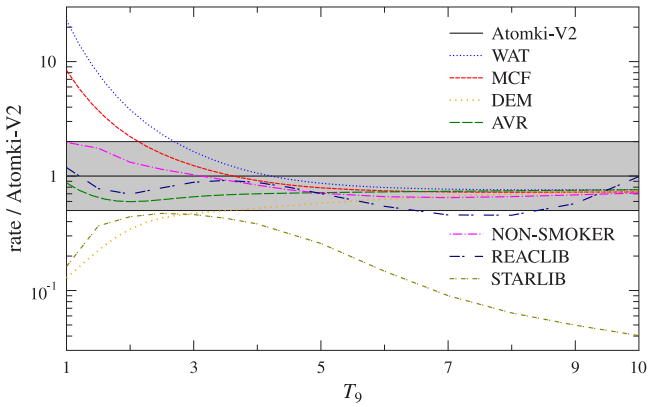

Fig. 8. Astrophysical reaction rates for the $Z \rightarrow Z+2$ production of strontium from ^{88}Kr + α from different AOMPs, normalized to the result of the present work. (For references, colors, and linestyles see the previous Fig. 7). In addition, the rates from NON-SMOKER(web) [34], REACLIB [37], and STARLIB [38] are included. Note that the decrease of the STARLIB rate at higher temperatures results from the fact that STARLIB provides the rate for the (α,1n) channel only. See the text for a more detailed discussion.

located between about 4 and 10 MeV for temperatures $1.5 \leq T_9 \leq 4$; here the predictions vary less dramatic. This is a typical finding for intermediate mass nuclei.

As a consequence, the predicted $Z \rightarrow Z+2$ reaction rates $N_A\langle\sigma v\rangle$ for ^{88}Kr + α vary over a less dramatic range than for ^{188}Sm + α (see Fig. 8). At the lowest temperatures the rates from the WAT and MCF AOMPs are about one order of magnitude above the present calculation. At $T_9 = 3$ all AOMPs predict a rate within a factor of two up or down from the present result. At higher temperatures, the STARLIB rate drops significantly which is again caused by the neglect of the (α,2n) channel (see above discussion for ^{188}Sm).

5. Discussion and presentation of the results

This study presents astrophysical reaction rates $N_A\langle\sigma v\rangle$ for 4359 target nuclei between iron ($Z = 26$) and bismuth ($Z = 83$). For each nucleus, the TALYS output file "astrorate.tot" is provided. A prefix of the file name is used to identify the nucleus under study (e.g., "z062a188_astrorate.tot" for the example of ^{188}Sm + α in Section 4.1). The files are available as part of this paper. As an example, the "z062a188_astrorate.tot" file for ^{188}Sm + α is also listed in Tables 2–8.

In addition to the (α, X) reaction rates, the TALYS "astrorate.tot" files provide two further columns (see Table 2). The second column of the TALYS output file shows the calculated partition function $G(T)$ (normalized to the ground state); for a definition of $G(T)$, see e.g. Eq. (12) of [21]. Furthermore, column 7 shows the fission rate which is negligible for the nuclei under study.

For the first time, reaction rates for all individual exit channels are provided. To make full usage of these rates, astrophysical reaction networks have to be extended accordingly. As previously provided rates are often inclusive rates, the TALYS output files are complemented by the last two columns with the summed $Z \rightarrow Z+1$ and $Z \rightarrow Z+2$ rates. These inclusive rates can be used in a similar way as before. Note that the $Z \rightarrow Z+2$ rates contain not only the sum over all (α, xn) rates, but also the (α, γ) rate ($x = 0$).

As extremely neutron-rich nuclei are typically produced under conditions with or at least close to a (n, γ)-(γ,n) equilibrium, the usage of a simple reaction network in combination with the summed $Z \rightarrow Z+2$ reaction rate provides reasonable results for the production of $Z+2$ nuclei. However, the usage of the (α,1n) rates from STARLIB in such a reaction network leads to a dramatic underestimation of the $Z \rightarrow Z+2$ production rate by many orders of magnitude.

Fit functions for all rates are not given because of several reasons. First, the accuracy of the fits may be poor; see e.g. the discrepancy between the tabular NON-SMOKER(web) rate and the parametrized REACLIB rate in Fig. 4. This holds in particular for those rates which exceed the numerical calculation limits of TALYS only at few, typically high, temperatures. Second, nowadays the reaction network codes are able to use tabulated reaction rates directly; this approach should be preferred because it avoids any uncertainties from fitting procedures.

6. Summary

The present study provides astrophysical reaction rates of α-induced reactions for 4359 nuclei between iron ($Z = 26$) and bismuth ($Z = 83$) from the neutron-deficient side "north-west" of stability to the neutron-rich side "south-east" of stability on the chart of nuclides. The tabulated data include the total $Z \rightarrow Z+1$ and $Z \rightarrow Z+2$ rates, often somewhat inaccurately labeled (α,p) and (α,n) in rate compilations, and the rates of all individual exit channels, mainly of (α, xn) type. The new rates are based on the Atomki-V2 α-nucleus potential which is capable of reproducing experimental total reaction cross sections with small deviations far below a factor of two [18]. A similar uncertainty can be expected for the summed $Z \rightarrow Z+2$ reaction rates even for very neutron-rich nuclei whereas the rates for the individual (α, xn) reactions must remain more uncertain because no experimental data are available to verify the present calculations for neutron-rich nuclei.

Declaration of competing interest

The authors declare that they have no known competing financial interests or personal relationships that could have appeared to influence the work reported in this paper.

Acknowledgments

We thank E. Somorjai, T. Rauscher, and D. Galaviz for many fruitful discussions on α-induced cross sections and α-nucleus potentials and the Atomki IT department for their support in the calculations. This work was supported by NKFIH, Hungary (Gr. No. K134197, NN128072) and by the New National Excellence Program of the Ministry for Innovation and Technology, Hungary (ÚNKP-20-5-DE-2, ÚNKP-20-5-DE-297). G. G. Kiss and T. Szücs acknowledge support from the János Bolyai research fellowship of the Hungarian Academy of Sciences. A. Arcones, M. Jacobi, and A. Psaltis were supported by the ERC Starting Grant EUROPIUM-677912, Deutsche Forschungsgemeinschaft, Germany through SFB 1245, and Helmholtz Forschungsakademie Hessen für FAIR, Germany. This work has benefited from the COST Action ChETEC (CA16117) supported by COST (European Cooperation in Science and Technology).

Appendix A. Modifications to the TALYS code

The following changes have been made to the TALYS code (version 1.8) for the implementation of the Atomki-V2 potential. The option *alphaomp 9* was added to the already available 8 options for the AOMP in TALYS. The real part of the Atomki-V2 potential is calculated by a double-folding procedure using the code DFOLD [39] outside TALYS; it is provided as an external file *alphaomp9real.gnu* in the following format. The first two lines

summarize the properties of the folding potential; these lines are read by TALYS, but the content is not considered. The third line provides the root-mean-square radius $r_{\rm rms}$, divided by $A_T^{1/3}$; this number R_0 is taken as Coulomb radius: $R_C = R_0 \times A_T^{1/3}$. The next 800 lines list the potential in the following format: radius r in fm (steps of 0.025 fm) and nuclear potential $V_N(r)$ in MeV. The imaginary potential with depth $W_0 = 50$ MeV, radius $R = R_0 \times A_T^{1/3}$ with $R_0 = 1.0$ fm, and diffuseness $a = 0.1$ fm is hard-coded in the source code.

In detail, the following changes have been made to the source code of TALYS. The modified source files and the required *alphaomp9real.gnu* files for the nuclei under study are available at At. Data Nuclear Data Tables. Practically, the option *alphaomp 9* is treated similar to other folding potentials (*alphaomp 3,4,5*); however, the TALYS-internal folding procedure is skipped, and instead the externally calculated folding potential is read by TALYS.

A.1. checkvalue.f

The minor technical modifications to *checkvalue.f* allow to select *alphaomp 9* and to increase the number of segments (see Appendix A.5).

A.2. egridastro.f

TALYS uses a relatively coarse built-in temperature grid for the calculation of astrophysical reaction rates. A finer temperature grid is chosen here, and very low temperatures are omitted because of negligibly small reaction rates for α-induced reactions on intermediate mass and heavy target nuclei.

A.3. endfenergies.f

The most relevant energies for astrophysical reaction rates are very low (compared to the recommended usage of TALYS up to 1 GeV). A finer energy grid is chosen here. For higher incoming energies, the increasing number of energy bins may lead to long computation times or even exceed the maximum number of bins (as defined in *talys.cmb*).

A.4. foldalpha.f

The main modification to the subroutine *foldalpha.f* allows to read an externally calculated folding potential *alphaomp9real.gnu* for the real part of the AOMP. Furthermore, the parameters of the imaginary part of the Atomki-V2 potential are given here.

A.5. grid.f

Here the resolution of the outgoing energy grid is enhanced for low energies. However, the resolution of the grid is reduced at high energies above 20 MeV. Consequently, the usage of this version is not recommended for high energies.

A.6. inputout.f

The technical modification to *inputout.f* provides the text "Atomki-V2" for the option *alphaomp 9*.

A.7. machine.f

The definition of the *machine.f* happens during the first installation of TALYS and depends on the available machine. As this is a user-specific file, *machine.f* is not provided here.

A.8. mainout.f

The technical modification to *mainout.f* provides a modified title "TALYS-1.8-Atomki-V2-partf-Tenh (V. 20210319 (PM)" for the TALYS output; it shows that the Atomki-V2 potential has been implemented and that the changes in the partition function (see Appendix A.10) and in the temperature grid of the reaction rates (see Appendix A.2) are active.

A.9. opticalcomp.f

The minor technical modification to *opticalcomp.f* is needed for the proper handling of the option *alphaomp 9*.

A.10. partfunc.f

There is a known problem in TALYS-V1.8 with the calculation of partition functions when the logarithmically binned energy grid is used. This problem was resolved in TALYS-V1.9. This *partfunc.f* is essentially taken from TALYS-V1.9. Equidistant binning was used in the present study to avoid any complications with the problem in TALYS-V1.8; the differences for the calculated reaction rates using equidistant or logarithmic binning are marginal as soon as the updated *partfunc.f* is used.

A.11. radialtable.f

The minor technical modification to *radialtable.f* is needed for the proper handling of the option *alphaomp 9*.

A.12. strucinitial.f

The minor technical modification to *strucinitial.f* is needed for the proper handling of the option *alphaomp 9*.

A.13. structure.f

The minor technical modification to *structure.f* is needed for the proper handling of the option *alphaomp 9*.

A.14. talys.cmb

The finer grid settings for the outgoing energy grid (see Appendix A.5) and the temperature grid for the reaction rates (see Appendix A.2) need to be reflected in the file *talys.cmb* with the general variable definitions.

Appendix B. Supplementary data

Supplementary material related to this article can be found online at https://doi.org/10.1016/j.adt.2021.101453.

References

[1] A. Coc, E. Vangioni, Internat. J. Modern Phys. E 26 (08) (2017) 1741002.
[2] C. Iliadis, Nuclear Physics of Stars, John Wiley & Sons, 2015.
[3] C.E. Rolfs, W.S. Rodney, Cauldrons in the Cosmos, The University of Chicago Press, Chicago, Illinois, USA, 1988.
[4] S.E. Woosley, W.M. Howard, Astrophys. J. Suppl. 36 (1978) 285–304.
[5] C. Travaglio, R. Gallino, T. Rauscher, F.K. Röpke, W. Hillebrandt, Astrophys. J. 799 (1) (2015) 54.
[6] D.L. Lambert, Astron. Astrophys. Rev. 3 (3–4) (1992) 201–256.
[7] T. Rauscher, N. Dauphas, I. Dillmann, C. Fröhlich, Z. Fülöp, G. Gyürky, Rep. Progr. Phys. 76 (6) (2013) 066201.
[8] M. Pignatari, K. Göbel, R. Reifarth, C. Travaglio, Internat. J. Modern Phys. E 25 (04) (2016) 1630003.
[9] N. Nishimura, T. Rauscher, R. Hirschi, A.S.J. Murphy, G. Cescutti, C. Travaglio, Mon. Not. R. Astron. Soc. 474 (3) (2017) 3133–3139.

[10] Z. Fülöp, Á.Z. Kiss, E. Somorjai, C.E. Rolfs, H.P. Trautvetter, T. Rauscher, H. Oberhummer, Z. Phys. A 355 (1996) 203–207.
[11] E. Somorjai, Z. Fülöp, A.Z. Kiss, C.E. Rolfs, H.P. Trautvetter, U. Greife, M. Junker, S. Goriely, M. Arnould, M. Rayet, T. Rauscher, H. Oberhummer, Astron. Astrophys. 333 (1998) 1112–1116.
[12] J. Bliss, A. Arcones, F. Montes, J. Pereira, J. Phys. G: Nucl. Part. Phys. 44 (5) (2017) 054003.
[13] J. Pereira, F. Montes, Phys. Rev. C 93 (2016) 034611.
[14] P. Mohr, Phys. Rev. C 94 (2016) 035801.
[15] J. Bliss, A. Arcones, F. Montes, J. Pereira, Phys. Rev. C 101 (2020) 055807.
[16] G.G. Kiss, T.N. Szegedi, P. Mohr, M. Jacobi, G. Gyürky, R. Huszánk, A. Arcones, Astrophys. J. 908 (2) (2021) 202.
[17] T. Szegedi, G. Kiss, G. Gyürky, P. Mohr, J. Phys. Conf. Ser. 1668 (2020) 012041.
[18] P. Mohr, Z. Fülöp, G. Gyürky, G.G. Kiss, T. Szücs, Phys. Rev. Lett. 124 (2020) 252701.
[19] J.J. Cowan, C. Sneden, J.E. Lawler, A. Aprahamian, M. Wiescher, K. Langanke, G. Martínez-Pinedo, F.-K. Thielemann, Rev. Modern Phys. 93 (2021) 015002.
[20] T. Rauscher, Internat. J. Modern Phys. E 20 (05) (2011) 1071–1169.
[21] T. Rauscher, F.-K. Thielemann, At. Data Nucl. Data Tables 75 (1) (2000) 1–351.
[22] G. Satchler, W. Love, Phys. Rep. 55 (3) (1979) 183–254.
[23] A.M. Kobos, B.A. Brown, R. Lindsay, G.R. Satchler, Nuclear Phys. A 425 (2) (1984) 205–232.
[24] H. Abele, G. Staudt, Phys. Rev. C 47 (1993) 742–756.
[25] P. Mohr, G. Kiss, Z. Fülöp, D. Galaviz, G. Gyürky, E. Somorjai, At. Data Nucl. Data Tables 99 (6) (2013) 651–679.
[26] T. Szücs, P. Mohr, G. Gyürky, Z. Halász, R. Huszánk, G.G. Kiss, T.N. Szegedi, Z. Török, Z. Fülöp, J. Phys. Conf. Ser. 1668 (1) (2020) 012042.
[27] A.J. Koning, S. Hilaire, S. Goriely, Computer code TALYS, version 1.8, 2017.
[28] U. Atzrott, P. Mohr, H. Abele, C. Hillenmayer, G. Staudt, Phys. Rev. C 53 (1996) 1336–1347.
[29] S. Watanabe, Nuclear Phys. 8 (1958) 484–492.
[30] L. McFadden, G.R. Satchler, Nuclear Phys. 84 (1) (1966) 177–200.
[31] P. Demetriou, C. Grama, S. Goriely, Nuclear Phys. A 707 (1) (2002) 253–276.
[32] V. Avrigeanu, M. Avrigeanu, C. Mănăilescu, Phys. Rev. C 90 (2014) 044612.
[33] P. Scholz, H. Wilsenach, H.W. Becker, A. Blazhev, F. Heim, V. Foteinou, U. Giesen, C. Münker, D. Rogalla, P. Sprung, A. Zilges, K. Zuber, Phys. Rev. C 102 (2020) 045811.
[34] T. Rauscher, Computer code NON-SMOKER(WEB), 2001.
[35] M. Beard, E. Uberseder, R. Crowter, M. Wiescher, Phys. Rev. C 90 (2014) 034619.
[36] T. Rauscher, Phys. Rev. C 81 (2010) 045807.
[37] R.H. Cyburt, A.M. Amthor, R. Ferguson, Z. Meisel, K. Smith, S. Warren, A. Heger, R.D. Hoffman, T. Rauscher, A. Sakharuk, H. Schatz, F.K. Thielemann, M. Wiescher, Astrophys. J. Suppl. Ser. 189 (1) (2010) 240.
[38] A.L. Sallaska, C. Iliadis, A.E. Champagne, S. Goriely, S. Starrfield, F.X. Timmes, Astrophys. J. Suppl. Ser. 207 (1) (2013) 18.
[39] H. Abele, P. Mohr, Computer code DFOLD, version 1.02, 2017.

Explanation of Tables

Table 1. List of target nuclei under study
Nuclide element, Z, A_{min}, A_{max}

Table 2. Astrophysical reaction rates $N_A\langle\sigma v\rangle$ (in cm^3 s^{-1} mole^{-1}) for the production of residual nuclei with $189 \leq A \leq 192$ from ^{188}Sm + α, including the partition function $G(T)$
$T9$ temperature in GK
$G(T)$ normalized partition function
nuc astrophysical production rates $N_A\langle\sigma v\rangle$ (in cm^3 s^{-1} mole^{-1}) for residual nuclei with $189 \leq A \leq 192$

Table 3. Astrophysical reaction rates $N_A\langle\sigma v\rangle$ (in cm^3 s^{-1} mole^{-1}) for the production of residual nuclei with $186 \leq A \leq 189$ from ^{188}Sm + α
$T9$ temperature in GK
nuc astrophysical production rates $N_A\langle\sigma v\rangle$ (in cm^3 s^{-1} mole^{-1}) for residual nuclei with $186 \leq A \leq 189$

Table 4. Astrophysical reaction rates $N_A\langle\sigma v\rangle$ (in cm^3 s^{-1} mole^{-1}) for the production of residual nuclei with $183 \leq A \leq 186$ from ^{188}Sm + α
$T9$ temperature in GK
nuc astrophysical production rates $N_A\langle\sigma v\rangle$ (in cm^3 s^{-1} mole^{-1}) for residual nuclei with $183 \leq A \leq 186$

Table 5. Astrophysical reaction rates $N_A\langle\sigma v\rangle$ (in cm^3 s^{-1} mole^{-1}) for the production of residual nuclei with $181 \leq A \leq 183$ from ^{188}Sm + α
$T9$ temperature in GK
nuc astrophysical production rates $N_A\langle\sigma v\rangle$ (in cm^3 s^{-1} mole^{-1}) for residual nuclei with $181 \leq A \leq 183$

Table 6. Astrophysical reaction rates $N_A\langle\sigma v\rangle$ (in cm^3 s^{-1} mole^{-1}) for the production of residual nuclei with $178 \leq A \leq 180$ from ^{188}Sm + α
$T9$ temperature in GK
nuc astrophysical production rates $N_A\langle\sigma v\rangle$ (in cm^3 s^{-1} mole^{-1}) for residual nuclei with $178 \leq A \leq 180$

Table 7. Astrophysical reaction rates $N_A\langle\sigma v\rangle$ (in cm^3 s^{-1} mole^{-1}) for the production of residual nuclei with $175 \leq A \leq 178$ from ^{188}Sm + α and the sum of the production of europium ($Z \rightarrow Z + 1$)
$T9$ temperature in GK
nuc astrophysical production rates $N_A\langle\sigma v\rangle$ (in cm^3 s^{-1} mole^{-1}) for residual nuclei with $175 \leq A \leq 178$

Table 8. Astrophysical reaction rates $N_A\langle\sigma v\rangle$ (in cm^3 s^{-1} mole^{-1}): sum of the production of gadolinium ($Z \rightarrow Z + 2$) from ^{188}Sm + α
$T9$ temperature in GK
nuc astrophysical production rates $N_A\langle\sigma v\rangle$ (in cm^3 s^{-1} mole^{-1}) for gadolinium ($Z \rightarrow Z + 2$)

Table 1
Range of nuclei under study.

Element	Z	A_{min}	A_{max}
Fe	26	42	90
Co	27	44	92
Ni	28	46	94
Cu	29	48	102
Zn	30	51	105
Ga	31	53	108
Ge	32	55	110
As	33	57	115
Se	34	59	118
Br	35	61	121
Kr	36	63	124
Rb	37	66	128
Sr	38	68	130
Y	39	70	132
Zr	40	72	134
Nb	41	74	136
Mo	42	77	144
Tc	43	79	147
Ru	44	81	150
Rh	45	83	152
Pd	46	86	154
Ag	47	88	156
Cd	48	90	163
In	49	92	165
Sn	50	94	169
Sb	51	97	172
Te	52	99	176
I	53	101	179
Xe	54	103	182
Cs	55	108	185
Ba	56	110	189
La	57	112	192
Ce	58	114	194
Pr	59	116	196
Nd	60	118	198
Pm	61	120	200
Sm	62	123	202
Eu	63	125	211
Gd	64	130	214
Tb	65	135	218
Dy	66	140	221
Ho	67	145	224
Er	68	149	227
Tm	69	150	230
Yb	70	151	234
Lu	71	154	237
Hf	72	150	240
Ta	73	152	242
W	74	154	244
Re	75	156	246
Os	76	158	248
Ir	77	160	250
Pt	78	162	252
Au	79	164	254
Hg	80	166	256
Tl	81	168	258
Pb	82	170	260
Bi	83	172	262

Table 2
Astrophysical reaction rates $N_A\langle\sigma v\rangle$ (in cm^3 s^{-1} mole^{-1}) for ^{188}Sm + α as a function of temperature: partition function $G(T)$ and production of residual nuclei with $189 \leq A \leq 192$.

# Reaction rate for 62 188Sm+a 46 reactions Jp(GS) = 0.0+								
T9	G(T)	(a,g)192Gd	(a,n)191Gd	(a,p)191Eu	(a,a)188Sm	Fission	190Gd	189Gd
0.1000	1.00000E+00	0.00000E+00	0.00000E+00	0.00000E+00	0.00000E+00	0.00000E+00	0.00000E+00	0.00000E+00
0.1500	1.00017E+00	0.00000E+00	0.00000E+00	0.00000E+00	0.00000E+00	0.00000E+00	0.00000E+00	0.00000E+00
0.2000	1.00252E+00	0.00000E+00	0.00000E+00	0.00000E+00	0.00000E+00	0.00000E+00	0.00000E+00	0.00000E+00
0.2500	1.01266E+00	0.00000E+00	0.00000E+00	0.00000E+00	0.00000E+00	0.00000E+00	0.00000E+00	0.00000E+00
0.3000	1.03721E+00	0.00000E+00	0.00000E+00	0.00000E+00	0.00000E+00	0.00000E+00	0.00000E+00	0.00000E+00
0.3500	1.08058E+00	0.00000E+00	0.00000E+00	0.00000E+00	0.00000E+00	0.00000E+00	0.00000E+00	0.00000E+00
0.4000	1.14418E+00	0.00000E+00	0.00000E+00	0.00000E+00	0.00000E+00	0.00000E+00	0.00000E+00	0.00000E+00
0.4500	1.22712E+00	0.00000E+00	0.00000E+00	0.00000E+00	0.00000E+00	0.00000E+00	0.00000E+00	0.00000E+00
0.5000	1.32729E+00	3.81735E−55	3.85659E−55	0.00000E+00	0.00000E+00	0.00000E+00	0.00000E+00	0.00000E+00
0.6000	1.56880E+00	4.81610E−50	5.16124E−50	0.00000E+00	0.00000E+00	0.00000E+00	0.00000E+00	0.00000E+00
0.7000	1.84871E+00	1.98460E−46	2.72024E−46	0.00000E+00	0.00000E+00	0.00000E+00	1.60729E−42	1.21437E−41
0.8000	2.15139E+00	9.80624E−44	2.96334E−43	0.00000E+00	6.17006E−51	0.00000E+00	4.77131E−39	4.66083E−38
0.9000	2.46619E+00	1.20590E−41	1.37185E−40	0.00000E+00	8.57024E−47	0.00000E+00	3.33296E−36	3.81908E−35
1.0000	2.78634E+00	6.01452E−40	2.70283E−38	0.00000E+00	1.85134E−43	0.00000E+00	7.75319E−34	1.02268E−32
1.2000	3.42839E+00	6.23162E−37	1.27416E−34	0.00000E+00	3.28769E−38	0.00000E+00	4.56039E−30	7.79931E−29
1.4000	4.06363E+00	4.91712E−34	8.86170E−32	0.00000E+00	3.74885E−34	0.00000E+00	3.86790E−27	8.16860E−26
1.6000	4.69169E+00	1.47429E−31	1.75097E−29	0.00000E+00	7.00350E−31	0.00000E+00	9.22268E−25	2.34098E−23
1.8000	5.31788E+00	2.17446E−29	1.47014E−27	4.49622E−51	3.62477E−28	0.00000E+00	9.56266E−23	2.96915E−21
2.0000	5.94997E+00	1.98763E−27	7.12083E−26	5.61526E−43	7.22907E−26	0.00000E+00	5.95688E−21	2.27806E−19
2.2500	6.76215E+00	2.68240E−25	5.44870E−24	3.48866E−38	1.96944E−23	0.00000E+00	5.95898E−19	2.70556E−17
2.5000	7.61734E+00	1.58053E−23	2.42035E−22	8.04774E−35	2.27204E−21	0.00000E+00	3.07609E−17	1.51371E−15
2.7500	8.53808E+00	4.65719E−22	6.19114E−21	4.46715E−32	1.34900E−19	0.00000E+00	8.51356E−16	4.36907E−14
3.0000	9.55119E+00	7.94869E−21	9.71432E−20	9.44187E−30	4.72260E−18	0.00000E+00	1.40210E−14	7.40714E−13
3.2500	1.06900E+01	8.83556E−20	1.01794E−18	9.53548E−28	1.07495E−16	0.00000E+00	1.52280E−13	8.25325E−12
3.5000	1.19980E+01	6.98514E−19	7.68839E−18	5.34128E−26	1.70987E−15	0.00000E+00	1.18565E−12	6.59563E−11
3.7500	1.35336E+01	4.19341E−18	4.45070E−17	1.84738E−24	2.00691E−14	0.00000E+00	7.05949E−12	4.03979E−10
4.0000	1.53793E+01	2.00731E−17	2.07130E−16	4.27284E−23	1.81226E−13	0.00000E+00	3.37701E−11	1.99389E−09
4.2500	1.76541E+01	7.94604E−17	8.03858E−16	7.02120E−22	1.30070E−12	0.00000E+00	1.34752E−10	8.23407E−09
4.5000	2.05362E+01	2.67278E−16	2.67443E−15	8.58707E−21	7.61179E−12	0.00000E+00	4.61343E−10	2.92504E−08
4.7500	2.42983E+01	7.79362E−16	7.78483E−15	8.10372E−20	3.70565E−11	0.00000E+00	1.38348E−09	9.11647E−08
5.0000	2.93677E+01	1.99891E−15	2.01161E−14	6.06938E−19	1.52454E−10	0.00000E+00	3.68743E−09	2.52650E−07
5.5000	4.65614E+01	9.30674E−15	9.75076E−14	1.85165E−17	1.63286E−09	0.00000E+00	1.90736E−08	1.40801E−06
6.0000	8.43197E+01	2.86434E−14	3.20814E−13	2.79375E−16	1.01234E−08	0.00000E+00	6.71142E−08	5.28277E−06
6.5000	1.75236E+02	6.16511E−14	7.49972E−13	2.33769E−15	3.92357E−08	0.00000E+00	1.67849E−07	1.39059E−05
7.0000	4.07280E+02	9.94307E−14	1.32235E−12	1.21584E−14	1.03810E−07	0.00000E+00	3.16535E−07	2.72700E−05
7.5000	1.01867E+03	1.28905E−13	1.87458E−12	4.36619E−14	2.04437E−07	0.00000E+00	4.80060E−07	4.25881E−05
8.0000	2.65517E+03	1.42134E−13	2.25258E−12	1.17683E−13	3.21305E−07	0.00000E+00	6.17966E−07	5.60304E−05
8.5000	7.06803E+03	1.38645E−13	2.38264E−12	2.52876E−13	4.23634E−07	0.00000E+00	7.01913E−07	6.46770E−05
9.0000	1.90093E+04	1.22837E−13	2.27637E−12	4.52062E−13	4.85056E−07	0.00000E+00	7.22435E−07	6.73614E−05
9.5000	5.13841E+04	1.00656E−13	2.00019E−12	6.93368E−13	4.94233E−07	0.00000E+00	6.86291E−07	6.45419E−05
10.0000	1.39269E+05	7.72991E−14	1.63804E−12	9.33813E−13	4.56301E−07	0.00000E+00	6.09731E−07	5.76895E−05

Table 3
Astrophysical reaction rates $N_A\langle\sigma v\rangle$ (in cm^3 s^{-1} mole^{-1}) for ^{188}Sm + α as a function of temperature: production of residual nuclei with $186 \leq A \leq 189$.

Reaction rate for 62 188Sm+a 46 reactions Jp(GS) = 0.0+

T9	189Eu	188Gd	188Eu	187Gd	187Eu	187Sm	186Gd	186Eu
0.1000	0.00000E+00	0.00000E+00	0.00000E+00	0.00000E+00	0.00000E+00	0.00000E+00	0.00000E+00	0.00000E+00
0.1500	0.00000E+00	0.00000E+00	0.00000E+00	0.00000E+00	0.00000E+00	0.00000E+00	0.00000E+00	0.00000E+00
0.2000	0.00000E+00	0.00000E+00	0.00000E+00	0.00000E+00	0.00000E+00	0.00000E+00	0.00000E+00	0.00000E+00
0.2500	0.00000E+00	0.00000E+00	0.00000E+00	0.00000E+00	0.00000E+00	0.00000E+00	0.00000E+00	0.00000E+00
0.3000	0.00000E+00	0.00000E+00	0.00000E+00	0.00000E+00	0.00000E+00	0.00000E+00	0.00000E+00	0.00000E+00
0.3500	0.00000E+00	0.00000E+00	0.00000E+00	0.00000E+00	0.00000E+00	0.00000E+00	0.00000E+00	0.00000E+00
0.4000	0.00000E+00	0.00000E+00	0.00000E+00	0.00000E+00	0.00000E+00	0.00000E+00	0.00000E+00	0.00000E+00
0.4500	0.00000E+00	0.00000E+00	0.00000E+00	0.00000E+00	0.00000E+00	0.00000E+00	0.00000E+00	0.00000E+00
0.5000	0.00000E+00	0.00000E+00	0.00000E+00	0.00000E+00	0.00000E+00	0.00000E+00	0.00000E+00	0.00000E+00
0.6000	0.00000E+00	0.00000E+00	0.00000E+00	0.00000E+00	0.00000E+00	0.00000E+00	0.00000E+00	0.00000E+00
0.7000	0.00000E+00	1.65914E−42	0.00000E+00	0.00000E+00	0.00000E+00	0.00000E+00	0.00000E+00	0.00000E+00
0.8000	0.00000E+00	1.07556E−38	0.00000E+00	0.00000E+00	0.00000E+00	0.00000E+00	0.00000E+00	0.00000E+00
0.9000	0.00000E+00	1.32011E−35	0.00000E+00	0.00000E+00	0.00000E+00	0.00000E+00	0.00000E+00	0.00000E+00
1.0000	0.00000E+00	5.22468E−33	0.00000E+00	0.00000E+00	0.00000E+00	0.00000E+00	0.00000E+00	0.00000E+00
1.2000	0.00000E+00	7.97116E−29	0.00000E+00	2.51817E−34	0.00000E+00	0.00000E+00	0.00000E+00	0.00000E+00
1.4000	6.69624E−41	1.52838E−25	0.00000E+00	1.18078E−28	0.00000E+00	0.00000E+00	1.26064E−32	0.00000E+00
1.6000	5.41228E−37	8.71891E−23	0.00000E+00	6.73221E−25	0.00000E+00	0.00000E+00	4.57922E−28	0.00000E+00
1.8000	7.25856E−34	2.50290E−20	9.63365E−41	6.00373E−22	0.00000E+00	8.88984E−42	1.29269E−24	0.00000E+00
2.0000	2.96257E−31	3.55376E−18	6.57282E−36	1.47236E−19	2.96447E−40	1.29850E−37	8.46599E−22	0.00000E+00
2.2500	1.64993E−28	6.20797E−16	5.41429E−32	3.98519E−17	1.23868E−34	4.55592E−34	6.47112E−19	0.00000E+00
2.5000	3.39961E−26	4.18697E−14	6.46554E−29	3.94965E−15	7.18534E−31	3.46548E−31	1.51545E−16	4.12276E−41
2.7500	3.28873E−24	1.37124E−12	2.36526E−26	1.90366E−13	6.70344E−28	9.49719E−29	1.49939E−14	6.30124E−34
3.0000	1.75412E−22	2.60549E−11	3.59289E−24	5.34231E−12	2.08049E−25	1.26048E−26	7.72570E−13	1.57269E−29
3.2500	5.73670E−21	3.27091E−10	2.74175E−22	9.82767E−11	2.92699E−23	9.68892E−25	2.37608E−11	2.25355E−26
3.5000	1.24166E−19	2.98131E−09	1.20186E−20	1.28561E−09	2.21007E−21	4.70448E−23	4.79112E−10	6.19101E−24
3.7500	1.88996E−18	2.11205E−08	3.33981E−19	1.26674E−08	1.00612E−19	1.51305E−21	6.79094E−09	7.22131E−22
4.0000	2.12678E−17	1.22068E−07	6.33722E−18	9.79943E−08	3.00648E−18	3.35503E−20	7.14569E−08	4.61312E−20
4.2500	1.84325E−16	5.95086E−07	8.69243E−17	6.13701E−07	6.28929E−17	5.33708E−19	5.83097E−07	1.83565E−18
4.5000	1.27150E−15	2.50157E−06	9.00820E−16	3.18490E−06	9.67486E−16	6.32329E−18	3.82102E−06	4.89892E−17
4.7500	7.16488E−15	9.19583E−06	7.30024E−15	1.39486E−05	1.13656E−14	5.76669E−17	2.06706E−05	9.25176E−16
5.0000	3.36588E−14	2.98217E−05	4.75235E−14	5.23037E−05	1.04978E−13	4.16181E−16	9.43254E−05	1.28939E−14
5.5000	4.57353E−13	2.20033E−04	1.13138E−12	4.82545E−04	4.74552E−12	1.17207E−14	1.25585E−03	1.14273E−12
6.0000	3.52438E−12	1.04319E−03	1.38397E−11	2.69879E−03	1.02668E−10	1.62955E−13	9.95642E−03	4.17767E−11
6.5000	1.68947E−11	3.34293E−03	9.71485E−11	9.87023E−03	1.19476E−09	1.26113E−12	5.10263E−02	7.39332E−10
7.0000	5.59058E−11	7.78470E−03	4.37795E−10	2.57440E−02	8.40707E−09	6.10807E−12	1.83963E−01	7.32753E−09
7.5000	1.41935E−10	1.42262E−02	1.40793E−09	5.20911E−02	3.98852E−08	2.05933E−11	5.04937E−01	4.62234E−08
8.0000	3.02533E−10	2.17267E−02	3.52364E−09	8.73571E−02	1.39279E−07	5.25523E−11	1.12212E+00	2.05209E−07
8.5000	5.77284E−10	2.89849E−02	7.32568E−09	1.27033E−01	3.82002E−07	1.07787E−10	2.10715E+00	6.90031E−07
9.0000	1.02095E−09	3.47775E−02	1.32698E−08	1.64934E−01	8.62875E−07	1.85312E−10	3.44189E+00	1.85331E−06
9.5000	1.69005E−09	3.82543E−02	2.16611E−08	1.94857E−01	1.66345E−06	2.75210E−10	4.99144E+00	4.13595E−06
10.0000	2.60976E−09	3.90752E−02	3.25702E−08	2.12194E−01	2.81406E−06	3.61058E−10	6.52606E+00	7.90672E−06

Table 4
Astrophysical reaction rates $N_A\langle\sigma v\rangle$ (in cm^3 s^{-1} mole^{-1}) for ^{188}Sm + α as a function of temperature: production of residual nuclei with $183 \leq A \leq 186$.

Reaction rate for 62 188Sm+a 46 reactions Jp(GS)= 0.0+

T9	186Sm	185Gd	185Eu	185Sm	184Gd	184Eu	184Sm	183Gd
0.1000	0.00000E+00	0.00000E+00	0.00000E+00	0.00000E+00	0.00000E+00	0.00000E+00	0.00000E+00	0.00000E+00
0.1500	0.00000E+00	0.00000E+00	0.00000E+00	0.00000E+00	0.00000E+00	0.00000E+00	0.00000E+00	0.00000E+00
0.2000	0.00000E+00	0.00000E+00	0.00000E+00	0.00000E+00	0.00000E+00	0.00000E+00	0.00000E+00	0.00000E+00
0.2500	0.00000E+00	0.00000E+00	0.00000E+00	0.00000E+00	0.00000E+00	0.00000E+00	0.00000E+00	0.00000E+00
0.3000	0.00000E+00	0.00000E+00	0.00000E+00	0.00000E+00	0.00000E+00	0.00000E+00	0.00000E+00	0.00000E+00
0.3500	0.00000E+00	0.00000E+00	0.00000E+00	0.00000E+00	0.00000E+00	0.00000E+00	0.00000E+00	0.00000E+00
0.4000	0.00000E+00	0.00000E+00	0.00000E+00	0.00000E+00	0.00000E+00	0.00000E+00	0.00000E+00	0.00000E+00
0.4500	0.00000E+00	0.00000E+00	0.00000E+00	0.00000E+00	0.00000E+00	0.00000E+00	0.00000E+00	0.00000E+00
0.5000	0.00000E+00	0.00000E+00	0.00000E+00	0.00000E+00	0.00000E+00	0.00000E+00	0.00000E+00	0.00000E+00
0.6000	0.00000E+00	0.00000E+00	0.00000E+00	0.00000E+00	0.00000E+00	0.00000E+00	0.00000E+00	0.00000E+00
0.7000	0.00000E+00	0.00000E+00	0.00000E+00	0.00000E+00	0.00000E+00	0.00000E+00	0.00000E+00	0.00000E+00
0.8000	0.00000E+00	0.00000E+00	0.00000E+00	0.00000E+00	0.00000E+00	0.00000E+00	0.00000E+00	0.00000E+00
0.9000	0.00000E+00	0.00000E+00	0.00000E+00	0.00000E+00	0.00000E+00	0.00000E+00	0.00000E+00	0.00000E+00
1.0000	0.00000E+00	0.00000E+00	0.00000E+00	0.00000E+00	0.00000E+00	0.00000E+00	0.00000E+00	0.00000E+00
1.2000	0.00000E+00	0.00000E+00	0.00000E+00	0.00000E+00	0.00000E+00	0.00000E+00	0.00000E+00	0.00000E+00
1.4000	0.00000E+00	0.00000E+00	0.00000E+00	0.00000E+00	0.00000E+00	0.00000E+00	0.00000E+00	0.00000E+00
1.6000	0.00000E+00	0.00000E+00	0.00000E+00	0.00000E+00	0.00000E+00	0.00000E+00	0.00000E+00	0.00000E+00
1.8000	1.40130E−45	1.20859E−37	0.00000E+00	0.00000E+00	0.00000E+00	0.00000E+00	0.00000E+00	0.00000E+00
2.0000	8.72799E−41	1.92729E−28	0.00000E+00	0.00000E+00	0.00000E+00	0.00000E+00	0.00000E+00	0.00000E+00
2.2500	5.14249E−36	4.73503E−24	0.00000E+00	8.40779E−45	1.56883E−29	0.00000E+00	0.00000E+00	0.00000E+00
2.5000	9.00575E−33	7.32130E−21	0.00000E+00	2.60079E−39	1.87953E−24	0.00000E+00	4.20390E−45	0.00000E+00
2.7500	4.73167E−30	3.09362E−18	3.98262E−40	4.54138E−34	3.71625E−21	0.00000E+00	3.53018E−39	8.12603E−33
3.0000	1.14100E−27	5.13435E−16	4.11070E−33	6.50789E−31	1.57678E−18	0.00000E+00	1.03060E−33	9.37168E−25
3.2500	1.51085E−25	4.13618E−14	1.41800E−28	3.31431E−28	2.70060E−16	8.17325E−39	2.84648E−30	6.27431E−21
3.5000	1.21059E−23	1.87730E−12	1.55512E−25	7.97888E−26	2.33857E−14	8.15205E−32	1.31495E−27	2.63784E−18
3.7500	6.19317E−22	5.35386E−11	4.04304E−23	9.61705E−24	1.17213E−12	2.54045E−27	3.29567E−25	3.81900E−16
4.0000	2.11273E−20	1.04074E−09	4.21822E−21	6.43104E−22	3.74353E−11	3.92322E−24	4.18713E−23	2.82266E−14
4.2500	5.02177E−19	1.46648E−08	2.39821E−19	2.70796E−20	8.19312E−10	9.32174E−22	2.68438E−21	1.26360E−12
4.5000	8.66568E−18	1.56961E−07	8.72672E−18	7.67601E−19	1.29913E−08	7.91358E−20	1.07694E−19	3.75204E−11
4.7500	1.12505E−16	1.32250E−06	2.18518E−16	1.53708E−17	1.55784E−07	3.47959E−18	2.94093E−18	7.83441E−10
5.0000	1.13196E−15	9.01389E−06	3.95582E−15	2.26194E−16	1.46036E−06	9.95621E−17	5.75133E−17	1.20251E−08
5.5000	5.85071E−14	2.39913E−04	5.63170E−13	2.20193E−14	6.76304E−05	3.01984E−14	9.28982E−15	1.28388E−06
6.0000	1.39293E−12	3.35096E−03	3.13865E−11	8.68069E−13	1.50661E−03	3.12049E−12	5.68370E−13	5.62654E−05
6.5000	1.73597E−11	2.72149E−02	8.11928E−10	1.63221E−11	1.82808E−02	1.34923E−10	1.57287E−11	1.19032E−03
7.0000	1.28288E−10	1.42543E−01	1.13558E−08	1.69892E−10	1.36066E−01	2.90942E−09	2.30761E−10	1.40708E−02
7.5000	6.29746E−10	5.30331E−01	9.80588E−08	1.11513E−09	6.91700E−01	3.63419E−08	2.05956E−09	1.05595E−01
8.0000	2.24714E−09	1.51348E+00	5.80062E−07	5.11056E−09	2.61351E+00	2.95517E−07	1.24504E−08	5.55803E−01
8.5000	6.22418E−09	3.50109E+00	2.53644E−06	1.76101E−08	7.79983E+00	1.70436E−06	5.51380E−08	2.20562E+00
9.0000	1.40238E−08	6.82366E+00	8.66297E−06	4.81099E−08	1.91922E+01	7.42071E−06	1.89300E−07	6.94845E+00
9.5000	2.65966E−08	1.15202E+01	2.40753E−05	1.08330E−07	4.01592E+01	2.55515E−05	5.25293E−07	1.80459E+01
10.0000	4.35720E−08	1.72006E+01	5.61872E−05	2.07054E−07	7.31440E+01	7.21115E−05	1.21629E−06	3.97570E+01

Table 5
Astrophysical reaction rates $N_A\langle\sigma v\rangle$ (in cm^3 s^{-1} mole^{-1}) for ^{188}Sm + α as a function of temperature: production of residual nuclei with $181 \leq A \leq 183$.

# Reaction rate for 62 188Sm+a 46 reactions Jp(GS) = 0.0+								
T9	183Eu	183Sm	182Gd	182Eu	182Sm	181Gd	181Eu	181Sm
0.1000	0.00000E+00	0.00000E+00	0.00000E+00	0.00000E+00	0.00000E+00	0.00000E+00	0.00000E+00	0.00000E+00
0.1500	0.00000E+00	0.00000E+00	0.00000E+00	0.00000E+00	0.00000E+00	0.00000E+00	0.00000E+00	0.00000E+00
0.2000	0.00000E+00	0.00000E+00	0.00000E+00	0.00000E+00	0.00000E+00	0.00000E+00	0.00000E+00	0.00000E+00
0.2500	0.00000E+00	0.00000E+00	0.00000E+00	0.00000E+00	0.00000E+00	0.00000E+00	0.00000E+00	0.00000E+00
0.3000	0.00000E+00	0.00000E+00	0.00000E+00	0.00000E+00	0.00000E+00	0.00000E+00	0.00000E+00	0.00000E+00
0.3500	0.00000E+00	0.00000E+00	0.00000E+00	0.00000E+00	0.00000E+00	0.00000E+00	0.00000E+00	0.00000E+00
0.4000	0.00000E+00	0.00000E+00	0.00000E+00	0.00000E+00	0.00000E+00	0.00000E+00	0.00000E+00	0.00000E+00
0.4500	0.00000E+00	0.00000E+00	0.00000E+00	0.00000E+00	0.00000E+00	0.00000E+00	0.00000E+00	0.00000E+00
0.5000	0.00000E+00	0.00000E+00	0.00000E+00	0.00000E+00	0.00000E+00	0.00000E+00	0.00000E+00	0.00000E+00
0.6000	0.00000E+00	0.00000E+00	0.00000E+00	0.00000E+00	0.00000E+00	0.00000E+00	0.00000E+00	0.00000E+00
0.7000	0.00000E+00	0.00000E+00	0.00000E+00	0.00000E+00	0.00000E+00	0.00000E+00	0.00000E+00	0.00000E+00
0.8000	0.00000E+00	0.00000E+00	0.00000E+00	0.00000E+00	0.00000E+00	0.00000E+00	0.00000E+00	0.00000E+00
0.9000	0.00000E+00	0.00000E+00	0.00000E+00	0.00000E+00	0.00000E+00	0.00000E+00	0.00000E+00	0.00000E+00
1.0000	0.00000E+00	0.00000E+00	0.00000E+00	0.00000E+00	0.00000E+00	0.00000E+00	0.00000E+00	0.00000E+00
1.2000	0.00000E+00	0.00000E+00	0.00000E+00	0.00000E+00	0.00000E+00	0.00000E+00	0.00000E+00	0.00000E+00
1.4000	0.00000E+00	0.00000E+00	0.00000E+00	0.00000E+00	0.00000E+00	0.00000E+00	0.00000E+00	0.00000E+00
1.6000	0.00000E+00	0.00000E+00	0.00000E+00	0.00000E+00	0.00000E+00	0.00000E+00	0.00000E+00	0.00000E+00
1.8000	0.00000E+00	0.00000E+00	0.00000E+00	0.00000E+00	0.00000E+00	0.00000E+00	0.00000E+00	0.00000E+00
2.0000	0.00000E+00	0.00000E+00	0.00000E+00	0.00000E+00	0.00000E+00	0.00000E+00	0.00000E+00	0.00000E+00
2.2500	0.00000E+00	0.00000E+00	0.00000E+00	0.00000E+00	0.00000E+00	0.00000E+00	0.00000E+00	0.00000E+00
2.5000	0.00000E+00	0.00000E+00	0.00000E+00	0.00000E+00	0.00000E+00	0.00000E+00	0.00000E+00	0.00000E+00
2.7500	0.00000E+00	0.00000E+00	0.00000E+00	0.00000E+00	0.00000E+00	0.00000E+00	0.00000E+00	0.00000E+00
3.0000	0.00000E+00	7.57122E−42	0.00000E+00	0.00000E+00	0.00000E+00	0.00000E+00	0.00000E+00	0.00000E+00
3.2500	0.00000E+00	6.72689E−36	2.60117E−25	0.00000E+00	8.96733E−41	0.00000E+00	0.00000E+00	0.00000E+00
3.5000	1.06165E−40	3.57757E−31	3.79478E−21	0.00000E+00	2.72228E−35	0.00000E+00	0.00000E+00	0.00000E+00
3.7500	1.43061E−32	3.74360E−28	2.50975E−18	0.00000E+00	2.49023E−30	1.35637E−26	0.00000E+00	2.59941E−42
4.0000	1.72048E−27	1.39548E−25	3.94542E−16	1.16868E−42	2.32949E−27	2.34805E−21	0.00000E+00	7.18874E−36
4.2500	4.16646E−24	2.65438E−23	2.78079E−14	1.94571E−33	7.92588E−25	3.21657E−18	3.64338E−44	1.33641E−30
4.5000	1.49750E−21	2.31756E−21	1.18878E−12	1.57656E−27	1.46695E−22	6.11985E−16	1.00427E−33	4.79522E−27
4.7500	1.41084E−19	1.00290E−19	3.40592E−11	6.38977E−24	1.18674E−20	4.04275E−14	5.77236E−28	2.09082E−24
5.0000	6.60407E−18	2.84174E−18	6.95684E−10	3.63466E−21	4.90279E−19	1.51825E−12	4.93316E−24	3.85535E−22
5.5000	3.72261E−15	8.47314E−16	1.22666E−07	2.60960E−17	2.40567E−16	6.76028E−10	6.43796E−19	1.93755E−18
6.0000	6.16395E−13	8.54947E−14	8.26952E−06	1.23503E−14	3.62248E−14	9.57152E−08	1.18020E−15	7.39031E−16
6.5000	4.01291E−11	3.58733E−12	2.55014E−04	1.51634E−12	2.17284E−12	5.50803E−06	2.53704E−13	8.15616E−14
7.0000	1.24824E−09	7.47594E−11	4.21257E−03	7.90865E−11	6.28555E−11	1.55120E−04	1.94198E−11	3.89467E−12
7.5000	2.17276E−08	9.00070E−10	4.27018E−02	2.13303E−09	1.02627E−09	2.49358E−03	7.10756E−10	9.67310E−11
8.0000	2.39200E−07	7.04123E−09	2.95235E−01	3.42165E−08	1.06776E−08	2.57756E−02	1.49389E−08	1.43489E−09
8.5000	1.82191E−06	3.90107E−08	1.50339E+00	3.61131E−07	7.73409E−08	1.86919E−01	2.01044E−07	1.40677E−08
9.0000	1.02493E−05	1.62953E−07	5.95790E+00	2.69987E−06	4.15826E−07	1.01294E+00	1.86928E−06	9.81912E−08
9.5000	4.47082E−05	5.37653E−07	1.91338E+01	1.51095E−05	1.74039E−06	4.29850E+00	1.27118E−05	5.15859E−07
10.0000	1.56981E−04	1.45227E−06	5.13503E+01	6.60454E−05	5.88122E−06	1.48042E+01	6.60747E−05	2.12891E−06

Table 6
Astrophysical reaction rates $N_A\langle\sigma v\rangle$ (in cm^3 s^{-1} mole^{-1}) for ^{188}Sm + α as a function of temperature: production of residual nuclei with $178 \leq A \leq 180$.

# Reaction rate for 62 188Sm+a 46 reactions Jp(GS) = 0.0+								
T9	180Gd	180Eu	180Sm	179Gd	179Eu	179Sm	178Gd	178Eu
0.1000	0.00000E+00	0.00000E+00	0.00000E+00	0.00000E+00	0.00000E+00	0.00000E+00	0.00000E+00	0.00000E+00
0.1500	0.00000E+00	0.00000E+00	0.00000E+00	0.00000E+00	0.00000E+00	0.00000E+00	0.00000E+00	0.00000E+00
0.2000	0.00000E+00	0.00000E+00	0.00000E+00	0.00000E+00	0.00000E+00	0.00000E+00	0.00000E+00	0.00000E+00
0.2500	0.00000E+00	0.00000E+00	0.00000E+00	0.00000E+00	0.00000E+00	0.00000E+00	0.00000E+00	0.00000E+00
0.3000	0.00000E+00	0.00000E+00	0.00000E+00	0.00000E+00	0.00000E+00	0.00000E+00	0.00000E+00	0.00000E+00
0.3500	0.00000E+00	0.00000E+00	0.00000E+00	0.00000E+00	0.00000E+00	0.00000E+00	0.00000E+00	0.00000E+00
0.4000	0.00000E+00	0.00000E+00	0.00000E+00	0.00000E+00	0.00000E+00	0.00000E+00	0.00000E+00	0.00000E+00
0.4500	0.00000E+00	0.00000E+00	0.00000E+00	0.00000E+00	0.00000E+00	0.00000E+00	0.00000E+00	0.00000E+00
0.5000	0.00000E+00	0.00000E+00	0.00000E+00	0.00000E+00	0.00000E+00	0.00000E+00	0.00000E+00	0.00000E+00
0.6000	0.00000E+00	0.00000E+00	0.00000E+00	0.00000E+00	0.00000E+00	0.00000E+00	0.00000E+00	0.00000E+00
0.7000	0.00000E+00	0.00000E+00	0.00000E+00	0.00000E+00	0.00000E+00	0.00000E+00	0.00000E+00	0.00000E+00
0.8000	0.00000E+00	0.00000E+00	0.00000E+00	0.00000E+00	0.00000E+00	0.00000E+00	0.00000E+00	0.00000E+00
0.9000	0.00000E+00	0.00000E+00	0.00000E+00	0.00000E+00	0.00000E+00	0.00000E+00	0.00000E+00	0.00000E+00
1.0000	0.00000E+00	0.00000E+00	0.00000E+00	0.00000E+00	0.00000E+00	0.00000E+00	0.00000E+00	0.00000E+00
1.2000	0.00000E+00	0.00000E+00	0.00000E+00	0.00000E+00	0.00000E+00	0.00000E+00	0.00000E+00	0.00000E+00
1.4000	0.00000E+00	0.00000E+00	0.00000E+00	0.00000E+00	0.00000E+00	0.00000E+00	0.00000E+00	0.00000E+00
1.6000	0.00000E+00	0.00000E+00	0.00000E+00	0.00000E+00	0.00000E+00	0.00000E+00	0.00000E+00	0.00000E+00
1.8000	0.00000E+00	0.00000E+00	0.00000E+00	0.00000E+00	0.00000E+00	0.00000E+00	0.00000E+00	0.00000E+00
2.0000	0.00000E+00	0.00000E+00	0.00000E+00	0.00000E+00	0.00000E+00	0.00000E+00	0.00000E+00	0.00000E+00
2.2500	0.00000E+00	0.00000E+00	0.00000E+00	0.00000E+00	0.00000E+00	0.00000E+00	0.00000E+00	0.00000E+00
2.5000	0.00000E+00	0.00000E+00	0.00000E+00	0.00000E+00	0.00000E+00	0.00000E+00	0.00000E+00	0.00000E+00
2.7500	0.00000E+00	0.00000E+00	0.00000E+00	0.00000E+00	0.00000E+00	0.00000E+00	0.00000E+00	0.00000E+00
3.0000	0.00000E+00	0.00000E+00	0.00000E+00	0.00000E+00	0.00000E+00	0.00000E+00	0.00000E+00	0.00000E+00
3.2500	0.00000E+00	0.00000E+00	0.00000E+00	0.00000E+00	0.00000E+00	0.00000E+00	0.00000E+00	0.00000E+00
3.5000	0.00000E+00	0.00000E+00	0.00000E+00	0.00000E+00	0.00000E+00	0.00000E+00	0.00000E+00	0.00000E+00
3.7500	0.00000E+00	0.00000E+00	0.00000E+00	0.00000E+00	0.00000E+00	0.00000E+00	0.00000E+00	0.00000E+00
4.0000	0.00000E+00	0.00000E+00	7.59406E−41	0.00000E+00	0.00000E+00	0.00000E+00	0.00000E+00	0.00000E+00
4.2500	3.54060E−24	0.00000E+00	6.82556E−35	0.00000E+00	0.00000E+00	0.00000E+00	0.00000E+00	0.00000E+00
4.5000	7.89969E−20	0.00000E+00	2.53054E−29	9.60352E−32	0.00000E+00	1.64218E−40	0.00000E+00	0.00000E+00
4.7500	4.71806E−17	1.40130E−44	3.01628E−26	4.17612E−23	0.00000E+00	1.69618E−34	0.00000E+00	0.00000E+00
5.0000	6.14581E−15	5.13840E−34	9.16823E−24	3.99510E−19	0.00000E+00	2.65840E−29	6.38835E−26	0.00000E+00
5.5000	8.76136E−12	6.02837E−24	1.95529E−19	2.49965E−14	1.18039E−30	2.37823E−23	1.77839E−17	7.00649E−45
6.0000	2.38077E−09	2.11864E−18	1.78337E−16	2.64717E−11	7.71138E−22	7.35261E−19	3.14485E−13	2.61974E−28
6.5000	2.24586E−07	3.02141E−15	3.00659E−14	4.76186E−09	2.79045E−17	5.41087E−16	1.54527E−10	2.42885E−21
7.0000	9.64802E−06	6.61586E−13	1.97331E−12	3.32661E−07	3.12256E−14	7.11302E−14	1.98239E−08	2.13916E−16
7.5000	2.24180E−04	4.00030E−11	6.45873E−11	1.14716E−05	3.42259E−12	3.52113E−12	9.90918E−07	7.49096E−14
8.0000	3.20924E−03	1.19427E−09	1.23292E−09	2.30813E−04	1.23416E−10	9.29777E−11	2.64579E−05	3.06151E−12
8.5000	3.11050E−02	2.15749E−08	1.52293E−08	3.00876E−03	2.58994E−09	1.51272E−09	4.38307E−04	7.08621E−11
9.0000	2.18548E−01	2.56617E−07	1.31209E−07	2.73450E−02	3.47266E−08	1.64718E−08	4.87360E−03	1.02738E−09
9.5000	1.17084E+00	2.14371E−06	8.34120E−07	1.83025E−01	3.19563E−07	1.27776E−07	3.86201E−02	1.00733E−08
10.0000	4.97050E+00	1.32339E−05	4.08644E−06	9.41132E−01	2.13484E−06	7.41340E−07	2.28678E−01	7.09073E−08

Table 7
Astrophysical reaction rates $N_A\langle\sigma v\rangle$ (in cm^3 s^{-1} mole^{-1}) for ^{188}Sm + α as a function of temperature: production of residual nuclei with $175 \leq A \leq 178$ and the sum of the production of europium ($Z \rightarrow Z + 1$).

Reaction rate for 62 188Sm+a 46 reactions Jp(GS) = 0.0+

T9	178Sm	177Gd	177Eu	177Sm	176Gd	176Sm	175Gd	Z+1-sum-Eu
0.1000	0.00000E+00	0.00000E+00	0.00000E+00	0.00000E+00	0.00000E+00	0.00000E+00	0.00000E+00	0.00000E+00
0.1500	0.00000E+00	0.00000E+00	0.00000E+00	0.00000E+00	0.00000E+00	0.00000E+00	0.00000E+00	0.00000E+00
0.2000	0.00000E+00	0.00000E+00	0.00000E+00	0.00000E+00	0.00000E+00	0.00000E+00	0.00000E+00	0.00000E+00
0.2500	0.00000E+00	0.00000E+00	0.00000E+00	0.00000E+00	0.00000E+00	0.00000E+00	0.00000E+00	0.00000E+00
0.3000	0.00000E+00	0.00000E+00	0.00000E+00	0.00000E+00	0.00000E+00	0.00000E+00	0.00000E+00	0.00000E+00
0.3500	0.00000E+00	0.00000E+00	0.00000E+00	0.00000E+00	0.00000E+00	0.00000E+00	0.00000E+00	0.00000E+00
0.4000	0.00000E+00	0.00000E+00	0.00000E+00	0.00000E+00	0.00000E+00	0.00000E+00	0.00000E+00	0.00000E+00
0.4500	0.00000E+00	0.00000E+00	0.00000E+00	0.00000E+00	0.00000E+00	0.00000E+00	0.00000E+00	0.00000E+00
0.5000	0.00000E+00	0.00000E+00	0.00000E+00	0.00000E+00	0.00000E+00	0.00000E+00	0.00000E+00	0.00000E+00
0.6000	0.00000E+00	0.00000E+00	0.00000E+00	0.00000E+00	0.00000E+00	0.00000E+00	0.00000E+00	0.00000E+00
0.7000	0.00000E+00	0.00000E+00	0.00000E+00	0.00000E+00	0.00000E+00	0.00000E+00	0.00000E+00	0.00000E+00
0.8000	0.00000E+00	0.00000E+00	0.00000E+00	0.00000E+00	0.00000E+00	0.00000E+00	0.00000E+00	0.00000E+00
0.9000	0.00000E+00	0.00000E+00	0.00000E+00	0.00000E+00	0.00000E+00	0.00000E+00	0.00000E+00	0.00000E+00
1.0000	0.00000E+00	0.00000E+00	0.00000E+00	0.00000E+00	0.00000E+00	0.00000E+00	0.00000E+00	0.00000E+00
1.2000	0.00000E+00	0.00000E+00	0.00000E+00	0.00000E+00	0.00000E+00	0.00000E+00	0.00000E+00	0.00000E+00
1.4000	0.00000E+00	0.00000E+00	0.00000E+00	0.00000E+00	0.00000E+00	0.00000E+00	0.00000E+00	6.69624E−41
1.6000	0.00000E+00	0.00000E+00	0.00000E+00	0.00000E+00	0.00000E+00	0.00000E+00	0.00000E+00	5.41228E−37
1.8000	0.00000E+00	0.00000E+00	0.00000E+00	0.00000E+00	0.00000E+00	0.00000E+00	0.00000E+00	7.25856E−34
2.0000	0.00000E+00	0.00000E+00	0.00000E+00	0.00000E+00	0.00000E+00	0.00000E+00	0.00000E+00	2.96264E−31
2.2500	0.00000E+00	0.00000E+00	0.00000E+00	0.00000E+00	0.00000E+00	0.00000E+00	0.00000E+00	1.65047E−28
2.5000	0.00000E+00	0.00000E+00	0.00000E+00	0.00000E+00	0.00000E+00	0.00000E+00	0.00000E+00	3.40615E−26
2.7500	0.00000E+00	0.00000E+00	0.00000E+00	0.00000E+00	0.00000E+00	0.00000E+00	0.00000E+00	3.31305E−24
3.0000	0.00000E+00	0.00000E+00	0.00000E+00	0.00000E+00	0.00000E+00	0.00000E+00	0.00000E+00	1.79213E−22
3.2500	0.00000E+00	0.00000E+00	0.00000E+00	0.00000E+00	0.00000E+00	0.00000E+00	0.00000E+00	6.04017E−21
3.5000	0.00000E+00	0.00000E+00	0.00000E+00	0.00000E+00	0.00000E+00	0.00000E+00	0.00000E+00	1.38401E−19
3.7500	0.00000E+00	0.00000E+00	0.00000E+00	0.00000E+00	0.00000E+00	0.00000E+00	0.00000E+00	2.32532E−18
4.0000	0.00000E+00	0.00000E+00	0.00000E+00	0.00000E+00	0.00000E+00	0.00000E+00	0.00000E+00	3.06619E−17
4.2500	0.00000E+00	0.00000E+00	0.00000E+00	0.00000E+00	0.00000E+00	0.00000E+00	0.00000E+00	3.36219E−16
4.5000	0.00000E+00	0.00000E+00	0.00000E+00	0.00000E+00	0.00000E+00	0.00000E+00	0.00000E+00	3.19761E−15
4.7500	1.01830E−39	0.00000E+00	0.00000E+00	0.00000E+00	0.00000E+00	0.00000E+00	0.00000E+00	2.69781E−14
5.0000	2.02555E−33	0.00000E+00	0.00000E+00	0.00000E+00	0.00000E+00	0.00000E+00	0.00000E+00	2.03117E−13
5.5000	3.06608E−25	1.40961E−28	0.00000E+00	1.61705E−33	0.00000E+00	3.74976E−39	0.00000E+00	8.07412E−12
6.0000	3.44514E−20	1.07521E−17	1.39830E−35	1.02928E−24	1.57338E−24	7.79061E−28	0.00000E+00	1.96946E−10
6.5000	6.80147E−17	1.30231E−13	1.40078E−25	3.84453E−20	3.02517E−17	2.00586E−22	0.00000E+00	3.03689E−09
7.0000	2.41545E−14	1.15746E−10	9.20164E−19	2.19562E−16	7.17848E−13	6.34989E−18	2.20100E−18	3.18410E−08
7.5000	1.65814E−12	1.14305E−08	1.57890E−15	3.42287E−14	1.92494E−10	3.70478E−15	1.56559E−14	2.46674E−07
8.0000	5.25727E−11	4.04505E−07	6.80473E−14	1.30896E−12	7.71833E−09	1.53603E−13	6.90438E−13	1.51357E−06
8.5000	9.94748E−10	8.36636E−06	1.64482E−12	2.87236E−11	1.75961E−07	3.59651E−12	1.70034E−11	7.72906E−06
9.0000	1.22620E−08	1.10915E−04	2.47222E−11	3.98678E−10	2.51995E−06	5.26353E−11	2.59531E−10	3.39250E−05
9.5000	1.05318E−07	1.01161E−03	2.49881E−10	3.77000E−09	2.44583E−05	5.20108E−10	2.65725E−09	1.30453E−04
10.0000	6.64512E−07	6.71040E−03	1.80525E−09	2.57411E−08	1.70707E−04	3.68507E−09	1.94081E−08	4.43597E−04

Table 8
Astrophysical reaction rates $N_A\langle\sigma v\rangle$ (in $cm^3\ s^{-1}\ mole^{-1}$) for $^{188}Sm + \alpha$ as a function of temperature: the sum of the production of gadolinium ($Z \rightarrow Z + 2$).

# Reaction rate for 62 188Sm+a 46 reactions Jp(GS) = 0.0+	
T9	Z+2-sum-Gd
0.1000	0.00000E+00
0.1500	0.00000E+00
0.2000	0.00000E+00
0.2500	0.00000E+00
0.3000	0.00000E+00
0.3500	0.00000E+00
0.4000	0.00000E+00
0.4500	0.00000E+00
0.5000	7.67394E−55
0.6000	9.97734E−50
0.7000	1.54106E−41
0.8000	6.21356E−38
0.9000	5.47250E−35
1.0000	1.62268E−32
1.2000	1.62265E−28
1.4000	2.38510E−25
1.6000	1.12195E−22
1.8000	2.86954E−20
2.0000	3.93561E−18
2.2500	6.88948E−16
2.5000	4.75154E−14
2.7500	1.62115E−12
3.0000	3.29250E−11
3.2500	4.57576E−10
3.5000	4.81507E−09
3.7500	4.10446E−08
4.0000	2.94625E−07
4.2500	1.81574E−06
4.5000	9.70719E−06
4.7500	4.53867E−05
5.0000	1.87194E−04
5.5000	2.26881E−03
6.0000	1.86260E−02
6.5000	1.11200E−01
7.0000	5.14577E−01
7.5000	1.94436E+00
8.0000	6.23853E+00
8.5000	1.74946E+01
9.0000	4.38277E+01
9.5000	9.97757E+01
10.0000	2.09181E+02